

RESEARCH MEMORANDUM

LOW-SPEED LONGITUDINAL STABILITY AND LATERAL-CONTROL

CHARACTERISTICS OF A MODEL OF A 40° SWEPT-WING

FIGHTER-TYPE AIRPLANE AT A REYNOLDS

NUMBER OF 9×10^6

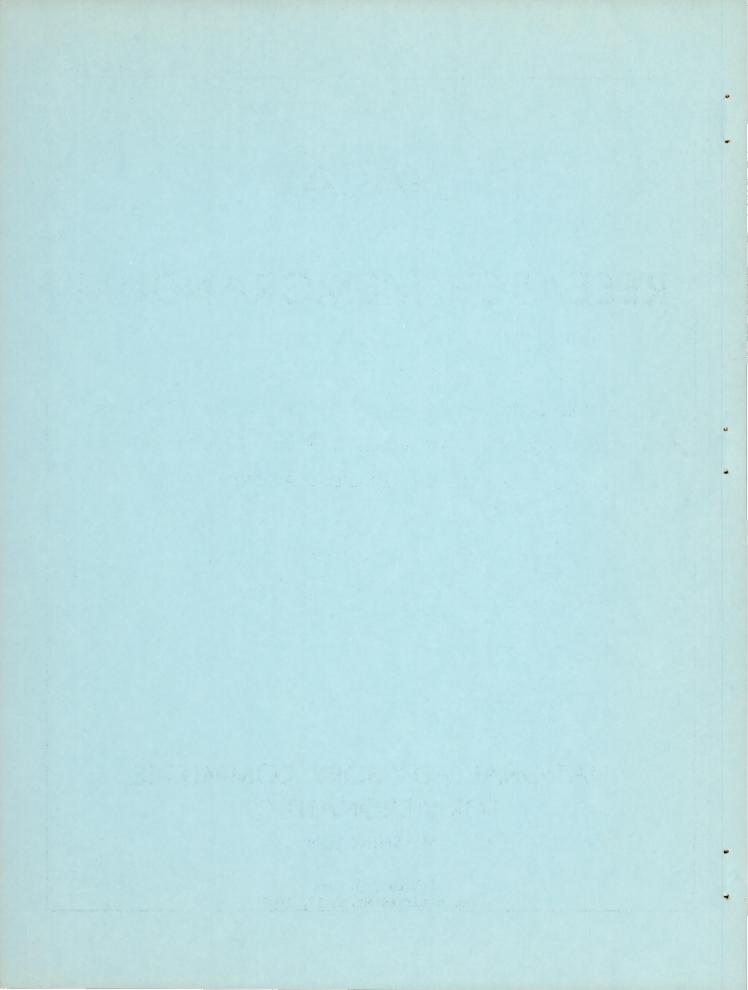
By Thomas V. Bollech and H. Neale Kelly

Langley Aeronautical Laboratory
Langley Field, Va.

NATIONAL ADVISORY COMMITTEE FOR AERONAUTICS

WASHINGTON

February 3, 1956 Declassified March 17, 1957



NATIONAL ADVISORY COMMITTEE FOR AERONAUTICS

RESEARCH MEMORANDUM

LOW-SPEED LONGITUDINAL STABILITY AND LATERAL-CONTROL CHARACTERISTICS OF A MODEL OF A 40° SWEPT-WING

FIGHTER-TYPE AIRPLANE AT A REYNOLDS

NUMBER OF 9 × 106

By Thomas V. Bollech and H. Neale Kelly

SUMMARY

An investigation was conducted in the Langley 19-foot pressure tunnel on a model of a 40° swept-wing fighter airplane to determine modifications which would eliminate the pitch-up that occurred near maximum lift during flight tests of the airplane. The effects of high-lift and stall-control devices, horizontal-tail locations, external stores, and various inlets on the longitudinal characteristics of the model were investigated. For the most part, these tests were conducted at a Reynolds number of 9.0×10^{6} and a Mach number of 0.19.

The results indicated that from the standpoint of stability the inlets should possess blunted side bodies. The horizontal tail located at either the highest or lowest position investigated improved the stability of the model. Three configurations were found for the model equipped with the production tail which eliminated the pitch-up through the lift range up to maximum lift and provided a stable static margin which did not vary more than 15 percent of the mean aerodynamic chord through the lift range up to 85 percent of maximum lift. The three configurations are as follows: The production wing-fuselage-tail combination with an inlet similar to the production inlet but smaller in plan form in conjunction with either (1) a wing fence located at 65 percent of the wing semispan or (2) an 11.7-percent chord leading-edge extension extending from 65.8 to 95.8 percent of the wing semispan and (3) the production wing-fuselage-tail combination with the production inlet and an 11.7-percent chord leading-edge extension extending from 70.8 to 95.8 percent of the wing semispan.

INTRODUCTION

The initial flight tests of a full-scale 40° swept-wing fighter airplane revealed that the airplane possessed undesirable pitch-up characteristics near maximum lift (at low as well as at high speeds). It was believed that the undesirable longitudinal stability characteristics were associated with the location of the horizontal tail on the airplane and the large shoulder-type inlets at the wing root.

In order to determine corrective modifications, a model of the airplane was tested in the Langley 19-foot pressure tunnel. The model was
employed to study the effects of: (1) changes in horizontal tail configuration (2) changes in wing root inlet configurations, and (3) miscellaneous
stall-control devices on the longitudinal stability characteristics of
the model.

In addition to the production tail, which had no dihedral and was located 28 percent of the semispan above the wing-chord plane extended, three alternate tail configurations were investigated. One tail configuration recommended by the Langley Laboratory was a drooped tail having -22° dihedral and utilizing the same point of attachment as the production tail. On the basis of an analysis using the downwash data of references 1 and 2, it was believed that this configuration would materially reduce or eliminate the high lift pitch-up. The other alternate tail configurations were obtained by attaching the production and the inverted drooped tail (22° dihedral) at the top of the vertical tail.

The effects of each of four pairs of inlets were investigated with the various horizontal tail arrangements to determine the effect of these configuration changes on the stability characteristics of the model. On the basis of these tests and from production considerations, an inlet which was similar to the production inlet but smaller in plan form was selected in conjunction with the production tail to be incorporated on the model for the investigation of stall-control devices on the longitudinal stability characteristics of the model. In addition, the effects of various wing devices on the longitudinal stability characteristics of the model equipped with the production inlet and tail were also determined.

A brief investigation was made to determine the lateral-control characteristics of the model equipped with the production inlet and tail and also of the model equipped with the production tail and an inlet similar to the production inlet but smaller in plan form.

The investigation reported herein was carried out for the most part at a Reynolds number of 9.0×10^6 and a Mach number of 0.19 through an angle-of-attack range from -4° to 30° . In an effort to determine the

effect of variation in Reynolds number, exploratory tests were made through a Reynolds number range from 2.2×10^6 to 11.0×10^6 . In order to expedite the issuance of these data, only a brief analysis has been made.

SYMBOLS

 c_L lift coefficient, $\frac{Lift}{q_o S_W}$

 c_{D} drag coefficient, $\frac{\mathrm{Drag}}{\mathrm{q_o S_W}}$

 $\begin{array}{c} c_m & \text{pitching-moment coefficient based on a center of gravity} \\ & \text{located at 2l percent \bar{c}} & \text{and 1.03 percent \bar{c}} \\ & \text{below fuselage center line,} & \frac{\text{Pitching moment}}{\text{qS}_{W}\bar{c}} \\ \end{array}$

 $\Delta C_{\rm m} = C_{\rm m} - \left[\alpha \left(\frac{dC_{\rm m}}{d\alpha} \right)_{\alpha=0} \right] - C_{\rm m}_{\alpha=0}$

 $\frac{dC_m}{dC_T}$ rate of change of pitching moment with lift coefficient

dC_m rate of change of pitching moment with angle of attack

 $\frac{dC_m}{di_+}$ rate of change of pitching moment with tail incidence

rolling-moment coefficient, corrected for model asymmetry, $\frac{\text{Rolling moment}}{q_{_{\mathbf{O}}}S_{_{\mathbf{W}}}b}$

yawing-moment coefficient, corrected for model asymmetry, $\frac{\text{Yawing moment}}{q_o S_W b}$

α angle of attack of wing chord plane, deg

it tail incidence angle in respect to the wing chord plane, deg

R Reynolds number based on the mean aerodynamic chord

q free-stream dynamic pressure, lb/sq ft

S_W projected wing area (excluding inlets), sq ft

 \bar{c} mean aerodynamic chord, $\frac{2}{S} \int_0^{b/2} c^2 dy$, ft

b wing span, ft

y spanwise distance measured from plane of symmetry, ft

z vertical distance above chord plane extended along mean aerodynamic chord, ft

 $\frac{V_1}{V_0}$ inlet velocity ratio, $\frac{Q}{AV_0}$

 $\left(\frac{H_e - P_o}{q_o}\right)$ exit total-pressure recovery

A inlet entrance area of both inlets, sq ft

H total pressure

P static pressure

Q volume rate of flow measured at fuselage exit, cu ft/sec

V velocity, ft/sec

Subscripts:

i inlet

e exit

o free stream

max maximum

l local

MODEL

The model of a 40° swept-wing fighter airplane installed in the Langley 19-foot pressure tunnel is shown in figure 1. The model was of steel-reinforced wood construction and its principal dimensions and design features are presented in figure 2 and table I. A rigging diagram of the model wing is presented in figure 3. The model was designed to allow tests of high-lift and stall-control devices, horizontal tail arrangements, external stores, and various inlets which varied in plan form.

The pertinent geometric characteristics of the inlets, devices, horizontal tail arrangements, and external stores are presented in figures 4 to 11 and tables II to VI.

The high-lift and stall-control devices consisted of plain trailingedge flaps, leading-edge extensions, wing fences, and a leading-edge modification which increased the leading-edge radius and camber of the wing sections thus modified.

The trailing-edge flaps extended to 51 percent of the semispan and had a chord of 22 percent of the wing chord measured parallel to the air stream. The flaps could be deflected 20° and 40° perpendicular to the hinge line (fig. 7).

The leading-edge extensions were designed so that any desired span, chord, or spanwise location could be investigated along with deflections of 0° and -10° measured in a plane perpendicular to the wing leading edge (fig. 6 and tables II, V, and VI).

Details of the leading-edge modification which increased the camber and leading-edge radius of the wing sections are shown in figure 7. The various wing fences are shown in figure 6 and tables II, V, and VI.

The various horizontal tail arrangements were comprised of either an undrooped or drooped tail (-22° dihedral) attached to the vertical tail at 28 percent of the wing semispan above the chord plane extended, and an undrooped or Y-tail, (22° dihedral) attached to the vertical tail at 65 percent of the wing semispan above the chord plane extended. The drooped and Y-tails had approximately 7 percent less projected area than the tails without any dihedral (fig. 5).

The model was equipped with partial and full-span ailerons which extended from 51 to 95.8 percent of the wing semispan and from 13.4 to 95.8 percent of the wing semispan, respectively. The model was also equipped for a few tests with solid and perforated flap-type spoilers which extended from 13.4 to 50 percent of the wing semispan and had an

average projection of 7.8 percent of the streamwise chord when deflected 90° (fig. 8). The area of the perforated spoiler was approximately 80 percent of the area of the solid spoiler. Unless otherwise indicated all lateral control tests were made with the ailerons or spoilers deflected on the left wing.

The model was provided with exhaust cones so that the inlet-exhaust area ratio could be varied, thus providing a means by which the mass flow ratio at the inlets could be varied (fig. 9). The stability data presented herein were obtained with the inlet exit full open. Flow survey rakes were installed at the approximate engine compressor face location and in the jet exit for the purpose of measuring flow rates at the above-mentioned locations (fig. 11).

Various boundary-layer diverter plates were provided on the model to study the effect of fuselage boundary layer on the internal-flow losses in the inlet. The boundary-layer diverter plates are shown in figure 10.

Designation of Test Configurations

Listed below are the designations of the basic component parts of the model:

A wing-fuselage-vertical-tail combination

B external stores (fig. 9)

Various inlets: (fig. 4)

D_O production inlet

D₁ inlet having a smaller plan form than D₀ with leading edge swept back 15°

D₂ D₁ with sidebody removed (simulated nacelle type)

D₃ semiflush inlet

 $D_{O_{C}}$ Do with spoiler on side body

 D_{0_1} D_0 with increased radius on side body

D_O vith approximate square side body

Horizontal tails: (fig. 5)

- T.28 production tail zero dihedral tail located at 28 percent of the wing semispan above the chord plane extended
- drooped tail similar to the production tail but having
 -22° dihedral located at 28 percent of the wing semispan
 above chord plane extended
- T-tail same as production tail but located at 65 percent of the wing semispan above chord plane extended
- Y-tail similar to the production tail but having 22° dihedral located at 65 percent of the wing semispan above the chord plane extended

High-lift and stall-control devices: (figs. 6 and 7)

- E leading-edge extensions (fig. 6)
- I leading-edge modification (fig. 7)
- F wing fences (fig. 6)
- δ_f trailing-edge flaps deflected (fig. 7)

Detail designations of the component parts are given in figures 4 to 9. The model configurations described herein are formed by combining the appropriate model components with the wing—fuselage—vertical-tail combination designated by the letter "A". For example, A + T $\overline{28}$ + B represents a wing—fuselage—vertical-tail combination plus zero dihedral horizontal tail located at 28 percent of the wing semispan above the chord plane extended plus external stores.

TESTS AND CORRECTIONS

Tests

The tests were conducted in the Langley 19-foot pressure tunnel with the air compressed in the tunnel to a pressure of approximately 33 pounds per square inch, absolute. With the exception of the wing—fuselage—vertical-tail combination, the investigation was carried out at a Reynolds number of 9.0 × 10⁶ and a Mach number of 0.19. In the case of the wing—fuselage—vertical-tail combination, force measurements were

obtained through a Reynolds number range from 2.2×10^6 to 11.0×10^6 . All tests were conducted over an angle-of-attack range from -4° to 31° .

Longitudinal characteristics of the model were determined for the model equipped with and without various inlets, high-lift and stall-control devices, horizontal tail arrangements, and with and without external stores. For the most part, the longitudinal stability tests were conducted with a horizontal tail incidence of -5°.

The lateral-control characteristics were determined through an aileron deflection range of ±18° by 3° increments for the outboard ailerons and ±12° by 3° increments for the inboard ailerons. In the case of the flap-type solid and perforated spoilers, deflections of 4.7°, 9.4°, 19°, 45°, 55°, and 90° were investigated. The aileron and spoiler deflections were measured in a plane perpendicular to their respective hinge lines.

Corrections

Corrections for wind-tunnel jet-boundary effects have been made to the pitching, rolling, and yawing moments. Corrections for support tare and interference have not been applied to the data. However, these corrections would not affect the comparisons of the data made herein. Jet-boundary corrections determined from reference 3 and air-flow-misalinement correction of 0.1°, estimated on the basis of air-flow surveys and tests of previous models, have been applied to the angle of attack and drag coefficient. The drag coefficients presented herein include the internal drag of the inlets.

PRESENTATION OF DATA

Tables II to VI summarize the results obtained from the low-speed longitudinal stability tests. Figures 12 to 34 present detail force and moment data of some of the more pertinent results obtained during the investigation of the longitudinal stability and lateral-control characteristics of the model. All of the stability data presented in figures 12 to 34 are for a tail incidence of approximately -5° unless otherwise noted. Tables VII and VIII present the individual ram-recovery pressures that were determined at the engine compressor face location for inlets D_1 and D_2 at several angles of attack and, in the case of inlet D_1 , for several boundary-layer diverter configurations. The variation of the mass-flow ratios and ram-recovery characteristics with angles of attack for the various inlets are presented in figures 35 and 36.

RESULTS AND DISCUSSION

Longitudinal Stability Characteristics

Effect of Reynolds number.- A few exploratory tests were conducted on the wing—fuselage—vertical-tail combination to determine the effects of Reynolds number. As indicated in figure 12, the effect of variation in Reynolds number on the pitching-moment characteristics of the wing—fuselage—vertical-tail combination from a Reynolds number of 5.0×10^6 to 11.0×10^6 can, for all practical purposes, be considered negligible. Although the effect of variation in Reynolds number on the pitching-moment characteristics of the wing—fuselage—vertical-tail combination was found to be small above a Reynolds number of 5.0×10^6 , it did not appear conclusive that the same would be true for all test configurations. Therefore, it was decided to conduct the investigation at the highest test Reynolds number possible with due consideration given to economy of operation and sustained operation of test equipment. Hence, the investigation was conducted at a Reynolds number of 9.0×10^6 rather than at the highest Reynolds number attainable of 11.0×10^6 .

Effect of inlets. With the exception of varying the length of the internal duct lines between the leading edge of the inlet and the leading edge of the wing, the internal ducting for the various inlets was designed to allow all of the various inlets to be installed on the model without altering the internal duct lines. It is assumed in the following discussion, therefore, that any variations which occur in the longitudinal characteristics of the model equipped with the different inlets are due entirely to the external effects of the inlets.

In order to show more clearly the effects of inlets on the pitching-moment characteristics of the model, figure 15 has been prepared, using the data of figure 13, and presents the departure of the pitching-moment curve from the initial linearity at low lift that was obtained for the model with and without the inlets. It was discovered during the initial phases of the investigation that the pitching-moment characteristics obtained on the model equipped with the production inlet D_0 were not in agreement with those obtained during the investigation of the full-scale airplane in the Ames 40- by 80-foot tunnel. It was recognized that the prototype inlet incorporated on the full-scale airplane differed from the production inlet on the model in that the prototype inlet possessed a sharper side body than the well-rounded side body of the production inlet. Therefore, in an effort to find an explanation for the discrepancy in the two sets of data, a spoiler was attached to the side

body of inlet D_0 in an attempt to simulate, to a reasonable extent, the aerodynamic effect of an inlet possessing a sharp side body. The results obtained with the simulated sharp side body inlet D_{0S} (fig. 13)

were found to be in sufficient agreement with the data obtained during the full-scale investigation to conclude that the differences that existed between the two sets of data obtained on the model and the full-scale airplane were attributable to the difference in the side body shapes of the prototype and the production inlets. It can be seen from the data presented in figure 15 that the addition of the simulated sharp side body inlet D_{OS} resulted in a maximum destabilizing pitching moment of 0.155 which was considerably greater than that obtained for the model without inlets. In addition the angle-of-attack range over which these increments of destabilizing pitching moment existed for inlet D_{OS} was considerably greater than for the model with inlets off. It is evident from the foregoing discussion that an inlet having a sharp side body would be detrimental to the longitudinal stability characteristics of the airplane.

Examination of figure 15 reveals that, with the exception of inlet D_3 , the addition of the inlets reduced to some extent the maximum increment of destabilizing pitching moment of approximately 0.111 that was obtained for the model without inlets at an angle of attack of approximately 21° . The greatest reduction, approximately 0.030, in the increment of destabilizing pitching moment was obtained with inlet D_2 . In the case of inlet D_3 (semiflush inlet) a slight increase in the maximum increment of destabilizing pitching moment was obtained. In addition, it can be seen that the increment of unstable pitching moment obtained for the model equipped with the various inlets and one fence progressively increased in magnitude and extended over a progressively larger angle-of-attack range as the inlet size increased.

Presented in figure 16 are the increments of destabilizing pitching moment obtained for the model equipped with various inlets and wing fences. Comparison of the data presented in figure 15 and figure 16 indicates that a properly located fence generally reduced the magnitude of the increments of destabilizing pitching moment by 75 percent for angles of attack below approximately 24°. It will also be noted from the data of figure 16 that the addition of one wing fence to the model equipped with inlet D₂, which has been previously shown to provide significant improvements in the pitching-moment characteristics, produced stable pitching-moment increments throughout the angle-of-attack range above 19°. Attempts to reduce further the magnitude and the extent of the increments of unstable pitching moment that occurred for model equipped with the larger inlets D₀ and D₀ by using two wing fences proved to be somewhat successful as can be seen from the data of figure 16. However, even with two fences the pitching-moment characteris-

tics of the model equipped with the larger inlets were still not as favorable as those obtained for the model equipped with inlet D₂ and only one fence.

Effect of horizontal tail location.— Presented in figure 17 are the longitudinal characteristics of the model equipped with various inlets and horizontal tail arrangements. The variations of dC_m/dC_L with lift coefficient obtained for the various inlet and horizontal tail arrangements are presented in figure 18. Inspection of figure 18 indicates that of the various horizontal tail arrangements investigated the Y-tail $\left(T_{.65}\right)$, regardless of the inlet configuration, was the only tail arrangement which provided negative values of dC_m/dC_L through the lift range up to $C_{I_{max}}$ or within 2 percent of $C_{I_{max}}$ in the case of inlet D_0 . However at or beyond $C_{I_{max}}$ the pitching-moment characteristics become unstable. In all cases, the variation of dC_m/dC_L with lift coefficient obtained with the Y-tail did not exceed 15 percent of the mean aerodynamic chord up to maximum lift. The smallest variation of dC_m/dC_L was obtained with inlet D_2 and was equal to $0.08\bar{c}$.

It can be seen from the data of figure 18 that decreasing the tail height by utilizing the drooped tail T $_{.28}^{\wedge}$ did not eliminate the positive values of dC_{m}/dC_{L} that occurred near $C_{L_{max}}$ with the production tail. However, the drooped tail sufficiently reduced the lift-coefficient range over which positive values of dC_{m}/dC_{L} occurred for the model equipped with the production tail so that in the case of inlets D_{2} and D_{1} it is probable that no pitch-up would be experienced in flight.

Examination of the relative merits of the various horizontal tail arrangements through a lift-coefficient range up to 0.85 $^{\rm C}{\rm L}_{\rm max}$ indicates that either the T $_{\rm c}^{\rm A}$ or the T $_{\rm c}^{\rm V}$ tail would provide negative values of dCm/dCL for all inlet configurations except for inlet D0 in conjunction with the drooped tail where positive values of dCm/dCL were obtained between a lift coefficient of 0.8 and 0.86. The variation of dCm/dCL that was obtained with the T $_{\rm c}^{\rm A}$ and T $_{\rm c}^{\rm V}$ tails through the usable lift range varied from 5 to 20 percent of the mean aerodynamic chord depending on the inlet configuration. The smallest variation of dCm/dCL through the usable lift range with the drooped tail was obtained with inlet D1 and was equal to 0.05c. In the case of the Y-tail the smallest variation of dCm/dCL was obtained with inlet D3 and was equal to 0.06c.

The values of dC_m/dit obtained at zero angles of attack for the various horizontal-tail locations are listed in the following table:

Horizontal-tail configuration	$\left(\frac{\mathrm{d}\mathbf{C}_{\mathrm{m}}/\mathrm{di}_{\mathrm{t}}}{\alpha}\right)_{\alpha=0}$
T.^	-0.0167
T.28	0187
T. 65	0190
T. 65	0177

^aDetermined from data of figure 17(a).

Effect of various wing devices on the model equipped with the production tail and inlets D_0 or D_1 . The effects of various arrangements or combinations of leading-edge extensions, wing fences and leading-edge modification on the stability characteristics of the model equipped with the production tail and inlets D_0 and D_1 were studied in an attempt to find a wing configuration which would provide stable pitching-moment characteristics through the lift-coefficient range.

As an aid in the selection of the most promising wing-device arrangement from the standpoint of stability, a criterion has been adopted that the model must not exhibit an adverse pitch-up tendency through the lift range up to $C_{\rm I_{max}}$ and must have a stable static margin which does not vary more than 15 percent of the mean aerodynamic chord through the lift-coefficient range up to 0.85 $C_{\rm I_{max}}$. It should be pointed out that this criterion was selected purely as a matter of convenience and should not be construed to mean that this criterion is a standard stability requirement. Also that the conclusions reached on the basis of this criterion may be somewhat altered if other criteria are used.

Of the many configurations investigated, several configurations were found which fulfilled the preceding requirements. These configurations are: (1) A + D₁ + T $\overline{.28}$ + 60 - F_{0.658}, (2) A + D₁ + T $\overline{.28}$ + E_{0.30}(0.658 - 0.958), and (3) A + D₀ + T $\overline{.28}$ + E_{0.25}(0.708 - 0.958). The detail force data obtained with these configurations with and without flaps deflected are presented in figure 19. The variations of dC_m/dC_L with lift coefficient for these configurations are presented in figure 20.

It is understood that the production version of the airplane is to be equipped with inlet D_0 , a leading-edge modification, and flight fences in conjunction with the straight tail located at 28 percent of the wing semispan above the chord plane extended, whereas the parasite version of the airplane will incorporate the droop tail. In light of this understanding, it is of interest to examine the detail force data obtained for the production and parasite versions of the airplane with flaps neutral and deflected (figs. 21 and 22). The variation of $dC_{\rm m}/dC_{\rm L}$ with lift coefficient obtained for these configurations is presented in figure 23. Figure 23 indicates that a pitch-up tendency would exist near $C_{L_{max}}$ with flaps neutral as well as flaps deflected for the production version. Drooping the horizontal tail 220 reduced the positive values of dC_m/dC_L near $C_{L_{max}}$ but the reduction was not sufficient to eliminate the pitch-up tendency. More significant than the reduction in the positive values of dC_m/dC_L that was obtained with the drooped tail is the loss in static margin that occurred. It will be noted from the data that drooping the horizontal tail decreased the static margin from approximately 10 to 6.5 percent c with flaps neutral and from approximately 10 to 5 percent c with flaps deflected.

Effect of external stores and inlet mass-flow ratios. The effect of external stores and inlet mass-flow ratio on the stability of the model for various model configurations is shown in figures 24 and 25. It can be seen that the addition of external stores had little effect on the linearity of the pitching-moment curves regardless of horizontal tail location or inlet configuration. However, it will be noted that a slight decrease in static margin was obtained in every case that the external stores were added.

Variations in the inlet mass-flow ratio appeared to have no effect on the stability of the model. The only significant effect of decreasing the inlet mass-flow ratio was a positive trim shift.

Lateral-Control Characteristics

Ailerons. The data presented in figures 26 and 27 indicate that the maximum values of rolling moment obtained with outboard ailerons was approximately 0.04 for a total aileron deflection of 36° for the model equipped with inlet D_1 and for the model equipped with inlet D_0 in conjunction with the leading-edge modification and flight fences. In both cases, a 25-percent decrease in rolling moment was obtained beyond an angle of attack of 16° . Furthermore, in the case of the model equipped with inlet D_0 in conjunction with the leading-edge modification and flight fences, the rolling-moment data became very erratic in nature, and in some instances, aileron reversal occurred.

Comparison of the results of figure 27 with those of figure 30 indicates that no significant change in the rolling moment was obtained by replacing the leading-edge modification and flight fences with an 11.7-percent chord leading-edge extension which extended from 70.8 to 95.8 percent of the wing semispan, (with flaps deflected in the latter case). However, when the outboard end of the extension was moved inboard to 0.858b/2 (fig. 31) a slight decrease in C_{lmax} was obtained and the variation of rolling moment with α above an angle of attack of 16° became less erratic with little or no aileron reversal. Although no data were obtained, it is reasonable to expect that an improvement

of 16° became less erratic with little or no aileron reversal. Although no data were obtained, it is reasonable to expect that an improvement in the variation of rolling moment with α would also be obtained with flaps neutral if the shortened span of leading-edge extension was employed.

The lateral-control data obtained on the model equipped with inlet D_0 , leading-edge modification and flight fences (fig. 28) indicate that the same degree of rolling effectiveness was obtained with 24° total deflection of the full-span ailerons as was obtained with 36° total deflection of the outboard ailerons. As in the case of outboard ailerons, the variation of rolling moment with α for the full-span ailerons above $\alpha = 16^{\circ}$ was erratic and in some instances aileron reversal was obtained. Therefore, as might be expected from the data obtained with full-span ailerons, it will be noted from a comparison of the data presented in figures 27 and 29 that the use of differentially operated flaps in conjunction with outboard ailerons as a lateral-control device appears to offer some advantage over outboard ailerons alone from the standpoint of rolling effectiveness.

Spoilers.— The lateral-control characteristics of 0.5b/2 span solid and perforated flap-type spoilers are presented in figures 32 and 33 for the model equipped with inlet D_0 , leading-edge modification, and flight fences. Comparison of the data presented in figures 32 and 33 reveals that at low angles of attack the rolling moment produced by either solid

or perforated spoilers deflected 55° was nearly equal to 50 percent of the rolling moment produced by an outboard flap-type aileron for a total aileron deflection of 18° . At high angles of attack both spoilers became ineffective. The variations of C_{l} with spoiler deflection at various angles of attack are presented in figure 34.

Thus it can be seen that spoilers were inferior to flap-type ailerons from the standpoint of rolling moment produced. It is probable that somewhat better spoiler effectiveness would be obtained with a more optimum spoiler arrangement.

The yawing-moment data obtained with flap-type ailerons and spoilers are in accordance with common experience in that the yawing moment produced by ailerons is generally unfavorable while that obtained with spoilers is favorable over most of the angle-of-attack range.

Internal Flow Measurements

Effect of boundary-layer diverters.— Figures 35 and 36 and tables VII and VIII present the internal flow measurements obtained on the model equipped with inlets D_1 and D_2 for several boundary-layer diverter configurations. The measurements were obtained for inlet velocity ratios which span the usual high-speed design inlet-velocity-ratio range from 0.6 to 0.8.

Examination of the data presented in figure 36 and tables VII and VIII indicates that replacing the original boundary-layer diverter block with splitter plates slightly improved the inlet air-flow characteristics. The greatest improvement was realized with the smaller of the two splitter plates investigated. The improvement that was obtained resulted from a decrease in the localized losses which occurred at the inner corners of the inlets.

CONCLUSIONS

An investigation has been conducted in the Langley 19-foot pressure tunnel at a Reynolds number of 9.0×10^6 on a model of a 40° swept-wing fighter airplane to determine modifications that would improve the low-speed longitudinal stability characteristics of the airplane. The lateral-control characteristics of the model were also determined.

From the results of the investigation, the following conclusions are made:

l. The addition of an inlet with a sharp side body increased the destabilizing pitching moment that occurred near $C_{\rm I_{max}}$ for the model without inlets, whereas a reduction in the destabilizing pitching moment was obtained with inlets having blunted side bodies. In addition the angle-of-attack range over which the increments of destabilizing pitching moment existed for the model equipped with a sharp side body inlet was considerably greater than for the model without inlets.

- 2. The horizontal tail located at either the highest or lowest position investigated during the present tests improved the stability of the model. The greatest improvement in stability associated with horizontal tail modification was obtained with a "Y" tail (22° dihedral) located at 65 percent of the wing semispan above the chord plane extended. This tail arrangement provided a stable static margin which did not vary more than 15 percent of the mean aerodynamic chord up to maximum lift or within 2 percent of maximum lift regardless of the inlet configuration. The drooped tail decreased the range of lift coefficient over which the pitch-up occurred to such an extent that it is probable that no pitch-up tendency would be experienced in flight.
- 3. Of all the arrangements of wing devices investigated on the model equipped with the production tail in conjunction with the production inlet or an inlet similar to the production inlet but smaller in plan form, three were found which eliminated the pitch-up and provided a stable static margin which did not vary more than 15 percent of the mean aerodynamic chord up to 85 percent of maximum lift. The three configurations are as follows: The production wing-fuselage-tail combination with an inlet similar to the production inlet but smaller in plan form, D₁, in conjunction with either, (1) one wing fence located at 65 percent of the wing semispan or, (2) an 11.7-percent chord leading-edge extension extending from 65.8 to 95.8 percent of the wing semispan, and (3) the production wing-fuselage-tail combination with the production inlet and an 11.7-percent chord leading-edge extension extending from 70.8 to 95.8 percent of the wing semispan.
- 4. The stability of the model was not affected appreciably by the addition of either external stores or a change in inlet velocity ratio.
- 5. Beyond an angle of attack of 16° which corresponds to approximately 80 percent of maximum lift, a 25-percent decrease in rolling moment was obtained for all flap-type ailerons investigated and in the case of the model equipped with the production inlet the rolling moment became very erratic in nature and in some instances aileron reversal was obtained. The addition of an 11.7-percent-chord leading-edge extension extending from 70.8 to 85.8 percent of the wing semispan resulted in rolling moments which were less erratic with angle of attack with little or no aileron reversal.

6. The rolling moment produced by a 50-percent-semispan solid or perforated flap-type spoiler deflected 55° was nearly equal to 50 percent of the rolling moment produced at low lift by an outboard flap-type aileron for a total aileron deflection of 18°. Beyond an angle of attack of 17°, however, both types of spoilers were ineffective.

Langley Aeronautical Laboratory,
National Advisory Committee for Aeronautics,
Langley Field, Va., February 1, 1954.

REFERENCES

- 1. Foster, Gerald V., and Griner, Roland F.: A Study of Several Factors Affecting the Stability Contributed by a Horizontal Tail at Various Vertical Positions on a Sweptback-Wing Airplane Model. NACA RM 19H19, 1949.
- 2. Salmi, Reino J.: Horizontal-Tail Effectiveness and Downwash Surveys for Two 47.7° Sweptback Wing-Fuselage Combinations With Aspect Ratios of 5.1 and 6.0 at a Reynolds Number of 6.0 × 10⁶. NACA RM L50K06, 1951.
- 3. Sivells, James C., and Salmi, Rachel M.: Jet-Boundary Corrections for Complete and Semispan Swept Wings in Closed Circular Wind Tunnels. NACA TN 2454, 1951.

TABLE I

GEOMETRIC CHARACTERISTICS OF THE MODEL

A. Wing Assembly

1. Basic data: Root airfoil (theoretical), measured normal to 0.25-chord line	NACA 64A010
Tip airfoil (theoretical), measured normal to	
0.25-chord line	NACA 64AO10
Angle of incidence, deg	
Geometric twist	
Sweep of quarter-chord line (true), deg	
Taper ratio	
Airfoil thickness (parallel to airplane center line	
percent c)	
Sweep of leading edge (true), deg	
Sweep of leading edge (projected), deg	
Cathedral, deg	
2. Dimensions: Root chord (theoretical), parallel to air stream .	
Tip chord (theoretical), parallel to air stream	
Mean aerodynamic chord	
Location of mean aerodynamic chord, spanwise (proje	cted) 27.126 in.
Span (projected)	
Span (true)	120.900 in.
3. Areas: Wing area (excluding inlet area), sq ft	20 250
Area of wing blanketed by fuselage, sq ft	

TABLE I .- Continued

GEOMETRIC CHARACTERISTICS OF THE MODEL

B. Horizontal Tail Assembly

1. Basic data:	
Root airfoil, measured normal to leading edge	NACA 64A009
Tip airfoil, measured normal to leading edge	NACA 64A009
Angle of incidence	Variable
Dihedral, deg	0
Sweepback (leading edge), deg	
Taper ratio	
Aspect ratio	3.59
2. Dimensions:	
Chord (constant)	
Mean aerodynamic chord	
Span	
Distance from 0.25c of wing to 0.25c of horizontal tail	69.356 in.
3. Areas:	
Total horizontal tail area, sq ft	5.022

GEOMETRIC CHARACTERISTICS OF THE MODEL

C. Vertical Tail Assembly	
1. Basic data: Airfoil, measured normal to 0.25-chord line	41.27
Taper ratio	0.402
Root chord (theoretical)	28.739 in. 10.500 in.
3. Areas: Vertical tail area, sq ft	3.861
D. Fuselage	
Location of station 0 (measured from nose of airplane), in	14.805
Maximum width	15.012 in.
Frontal area, sq ft	20.772 in. 1.749
Fineness ratio	8.59 14.499
Side area (excluding vertical tail), sq ft	18.558

GEOMETRIC CHARACTERISTICS OF THE MODEL

E. Inboard Flaps

1. Basic data:
Type
Angular travel, measured in a plane normal to
hinge line, deg
Location of inboard edge, measured normal to
fuselage center line
Location of outboard edge, measured normal to fuselage center line
Wing chord at inboard edge, measured parallel to
fuselage center line
fuselage center line
Location of hinge center line, measured normal
to 0.25-chord line
2. Dimensions:
Root chord, measured parallel to fuselage center line 9.29 in.
Tip chord, measured parallel to fuselage center line 7.78 in.
3. Area:
Area of one flap, sq ft

GEOMETRIC CHARACTERISTICS OF THE MODEL

F. Ailerons

1. Outboard ailerons:	
(a) Basic data:	
Type	Plain flap
Angular travel, measured in a plane normal to hinge	
line, deg	-18 to 18
Location of inboard edge, measured normal to fuselage	
center line	31.18 in.
Location of outboard edge, measured normal to fuselage	
center line	57.89 in.
Wing chord at inboard edge, measured parallel to fuselage	
center line	35.14 in.
Wing chord at outboard edge, measured parallel to fuselage	
center line	26.71 in.
Location of hinge center line, measured normal to	0.75c
0.25-chord line	0.170
(b) Dimensions:	7.70 in.
Root chord, measured parallel to fuselage center line	5.87 in.
Tip chord, measured parallel to fuselage center line	5.07 111.
(c) Area:	1 00
Area of one aileron, sq ft	1.29

GEOMETRIC CHARACTERISTICS OF THE MODEL

F. Ailerons (Cont.)

. Full-span ailerons:									
(a) Basic data									
Type	•	•			٠	•	P	Plai	n Flap
line, deg								-18	to 18
Location of inboard edge, measured normal to fuselage									
center line, in			 						9.36
Location of outboard edge, measured normal to fuselage									
center line, in			 						57.89
Wing chord at inboard edge, measured parallel to fuselage									
center line, in			 						41.65
Wing chord at outboard edge, measured parallel to fuselage									
center line, in									26.71
Location of hinge center line, measured normal to									
0.25-chord line			 						0.750
(b) Dimensions:									
Root chord, measured parallel to fuselage center line, in.									
Tip chord, measured parallel to fuselage center line, in.			 						5.87
(c) Area:									
Area of one aileron, sq ft									2.60

GEOMETRIC CHARACTERISTICS OF THE MODEL

F. Ailerons (Conc.)

3. Inboard spoilers:	
(a) Basic data	
Type	Flap
Angular travel, measured in a plane normal to hinge	
line, deg	90
Location of inboard edge, measured normal to fuselage	
center line, in	L.64
Location of outboard edge, measured normal to fuselage	
center line, in	L.14
Wing chord at inboard edge, measured parallel to fuselage	
	0.94
Wing chord at outboard edge, measured parallel to fuselage	
	+.97
Location of hinge center line, measured parallel to fuselage	
	.70c
(b) Dimensions	
	3.23
	2.75
(c) Area	
7 1	.37
4. Perforated Inboard Spoilers	
This section is exactly the same as 3 except for 3(c) which	
should be as follows:	
(c) Areas	
	.37
Area removed by perforation, sq ft	0.07

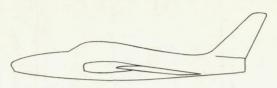
TABLE I.- Concluded

GEOMETRIC CHARACTERISTICS OF THE MODEL

i .	External Tanks (450-gallon capacity)	
	Diameter, in	5.47 8.81 0.42 4.25
	line, in	3.18
	Vertical location of nose of tank, measured normal to fuselage center line, in	5.69
	fuselage center line, in	1.25
	H. Pylons	
		30.0
	0011001 11110) 1100 1 1 1 1 1 1 1 1 1 1	30.0
	Chord, measured along line -2° from fuselage center line, in	7.04
	line, percent	7.25

TABLE II

 $\left[R = 9 \times 10^6\right]$



Parameter	Wing	Tail
Aspect ratio	3.49	
Taper ratio	0.58	_
Quarter-chord sweep, deg	40.8	_
Dihedral, deg	-3.5	_
Incidence, deg	-1.5	_
Airfoil section	64A010	_
Tail height, wing semispan		

nlet	T.E.	L.E. devi	ce		Fence configuration	C.	a at	Connva	Figure
	device	Туре	Span	Chord	Fence configuration CL	Lmax	C _{Lmax} ,	C _m curve	rigure
						.90	20.0	C _L 0 .h .8 1.2	12
						.88	20.0	C _m 1 (1) }	
D ₃						.89	20.0		
D ₂						.89	20.0		
D ₁						.90	21.0		
D ₁					2y/b = 0.658	1.01	21.0		
D ₁			_		2y/b = 0.708	•99	24.0		
D ₁	Plain Flap 0.139b/2 to 0.515b/2 8 = 40				2y/b = 0.658	1.09	18.2		
D ₁	Plain Flap 0.139b/2 to 0.515b/2 0 _f = 400				2y/b = 0.708	1.03	17.0		
D ₁	-	Chord-extension Normal leading-edge radius	0.658b/2 to 0.958b/2	0.1170	To the second	1.05	23.0		19
D ₁		Chord-extension Normal leading-edge radius	0.658b/2 to 0.808b/2	0.1170		1.01	23.0		

⁽¹⁾ Data obtained at $R = 2.2 \times 10^6$

TABLE II .- Continued

$$R = 9 \times 10^6$$

Tulat	T.E.	L.S. device			Fence configuration	C.	a at	C _m curve	Figur
nlet	device	Type	Span	Chord	ronco contiguidados	max	C _{L_{max},}	m date	0
D ₁	_	Chord-extension 2 × normai leading- edge radius	0.658b/2 to 0.808b/2	0.0590		•99	20.0	Cm1 CL .8 1.2	
D ₁		Chord-extension	0.658b/2 to 0.808b/2	0.029c		-97	20.0		
D ₁	_	Chord-extension Sharp leading edge	0.358b/2 to 0.508b/2	0.0590		.91	19.9		
D ₁	Plain Flap 0.139b/2 to 0.515b/2 0f = 20	Normal leading-edge	0.658b/2 to 0.958b/2	0.1170		1.09	20.0		
D ₁	Plain Flap 0.139b/2 to 0.515b/2 0f = 40	Chord-extension	0.658b/2 to 0.958b/2	0.1170		1.10	17.6		
D ₁	Plain Flap 0.139b/2 to 0.515b/2 0 = 40	Normal leading-edge	0.658b/2 to 0.808b/2	0.1170		1.06	17.0		19
D ₁	Plain Flap 0.139b/2 to 0.515b/2 0 = 40	2 × normal leading-	0.658b/2 to 0.808b/2	0.0590		1.08	17.0		
D ₁	Plain Flap 0.139b/2 to 0.515b/2 0 = 40		0.358b/2 to 0.508b/2	0.0590		1.05	14.0		
D ₁	_	Leading-edge modification 2 × normal leading- edge radius	0.652b/2 to 0.958b/2			•94	20.3		
D ₁	-	Leading-edge modification 2 × normal leading- edge radius	0.652b/2 to 0.802b/2			•94	20.9		
D ₁		Leading-edge modification 2 × normal leading- edge radius	0.652b/2 to 0.958b/2		2y/b = 0.658	•99	24.6		
D ₁		Leading-edge modification 2 × normal leading-edge radius (inboard end faired)	0.652b/2 to 0.958b/2		2y/b = 0.608 2y/b = 0.850	-94	21.4		
D ₁	Plain Flap 0.139b to 0.515b of = 40	modification	0.652b/2 to 0.958b/2		2 y/b = 0.658	1.02	24.0		

TABLE II. - Continued

$$\boxed{R = 9 \times 10^6}$$

-1-1	T.E.	L.E. devi	се		Panca configuration		a at	0	
inlet	device	Type	Span	Chord	Fence configuration	Lmax	CL _{max} ,	C _m curve	Figur
D _O	_		_			•96	24.8	C _m 0 .4 .8 1.2	
D _O	-				2y/b = 0.708 2y/b = 0.850	•97	23.0		
D _O	Plain Flap 0.139b/2 to 0.515b/2 8 = 409				2y/b = 0.708 2y/b = 0.850	1.03	23.0		
D _O	_	Chord-extension Normal leading-edge radius	0.708b/2 to 0.958b/2	0.1170		1.09	25.0		19
D ₀	_	Chord-extension Normal leading-edge radius	0.708b/2 to 0.858b/2	0.1170	-	1.08	24.0		
D _O	Plain Flap 0.139b/2 to 0.515b/2 0 = 40°	Chord-extension Normal leading-edge radius	0.708b/2 to 0.958b/2	0.1170		1.18	22.2		19
D ₀	Plain Flap 0.139b/2 to 0.515b/2 8 = 400	Chord-extension Normal leading-edge radius	0.708b/2 to 0.858b/2	0.1170		1.15	22.0		
D _O	_	Leading-edge modification 2 × normal leading-edge radius	0.708b/2 to 0.958b/2		2y/b = 0.708 2y/b = 0.850	•97	24.0		
Do		Leading-edge modification 2 × normal leading-edge radius	0.652b/2 to 0.958b/2		2y/b = 0.482 2y/b = 0.652	1.10	25.0		

TABLE II. - Concluded

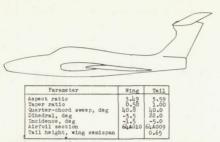
$$\left[R = 9 \times 10^6\right]$$

Inlet	T.E.	L.E. devi	ce		Wanga configuration		a at		
	device	Types	Span	Chord	Fence configuration	Lmax	C _{Lmax} ,	C _m curve	Figure
Do	Plain Flap 0.139b/2 to 0.515b/2 0 _f = 400	2 × normal leading-	0.708b/2 to 0.958b/2		2y/b = 0.708 $2y/b = 0.850$	1.03	31.0	C _L .8 1.2	
Do	Plain Flap 0.139b/2 to 0.515b/2 8 _f = 40°	Leading-edge modification 2 × normal leading- edge radius	0.652b/2 to 0.958b/2		2y/b = 0.482 $2y/b = 0.652$	1.10	22.5		
Do	Plain Flap 0.1390/2 to 0.515b/2 $\delta_{\mathbf{f}} = 40^{\circ}$	2 × normal leading-	0.652b/2 to 0.958b/2		2y/b = 0.482 2y/b = 0.652	1.12	24.0		

^{*}Highest angle of test

TABLE III

 $\left[R = 9 \times 10^6\right]$

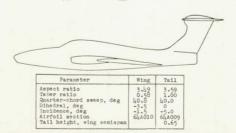


Inlet	T.E. device	L.E. de	vice		Danas sanki		a at.		
miec	device	Туре	Span	Chord	Pence configuration	Lmax	CLmax,	C _m curve	Figure
_				_		•95	19.8	C _m 1	17
D3	_					•95	21.0		17
D ₂	_			_		•94	20.2		17
D ₁						•95	20.8		17
Do	_		-	_		1.01	24.0		17

TABLE IV

SUMMARY OF LONGITUDINAL STABILITY CHARACTERISTICS, T-TAIL

 $\boxed{R = 9 \times 10^6}$



Inlet	T.E.	L.E. de	vice		Fence configuration		a at		
	device	Туре	3pan	Chord	rence configuration	Lmax	CLmax,	C _m curve	Figure
	-		_			•92	20.0	C _m 0 .4 .8 1.2	17

TABLE V

$$\left[R = 9 \times 10^{6}\right]$$



Parameter	Wing	Tail.
Aspect ratio Taper ratio Quarter-chord sweep, deg Dihedral, deg Incidence, deg Airfoil section Tail height, wing semispan	3.49 0.58 40.8 -3.5 -1.5 64A010	3.59 1.00 40.0 -5.0 64A009 0.28

				Open particular of		-			
Inlet	T.E. device	L.E. dev	Ice		Fence configuration	C _{Lme}	a at	C _m curve	Figure
		Туре	Span	Chord		III CX	deg.		
						•94	* 31.0	O .4 .8 1.2 .1 O C _m 1 2 3	13
D ₃						1.06	* 31.0		13
D ₂						•96	# 31.0		13
D ₂					2y/b = 0.658	1.03	24.0		14
P ₁	_					•96	# 31.0		13

^{*}Highest angle of test

TABLE V.- Continued

$$\boxed{R = 9 \times 10^6}$$

Inlei	T.E. device	L.S. 6	levice		Pence configuration		a at		L
1110	device	Туре	Span	Chord	Pence configuration	Lmax	CL _{max} ,	C _m curve	Figure
D ₁	Plain Plap 0.139b/2 - to 0.515b/2 8 _f = 40°		-	_		1.03	13.7	0 .4 .8 1.2 0 .1 .8 1.2 0 .1 .8 1.2	
D ₁			-		2y/b = 0.608	1.04	22.5		
D ₁					2y/b = 0.658	1.05	24.0	1	
D ₁	_		_		2y/b = 0.708	1.01	24.5		24
D ₁			_	_	h/t = 0.40 2y/b = 0.658	1.02	23.0	P	
D ₁	-				2y/b = 0.708	•97	# 31.0		
D ₁			_		2y/b = 0.658	1.00	22.2		
D ₁			-		2y/b = 0.658	1.01	22.2		

^{*}Highest angle of test

TABLE V.- Continued

$$\boxed{R = 9 \times 106}$$

Inlet	T.E. device	L.E. devi	lce		Fence configuration		a at		
mio	device	Туре	Span	Chord	Fence configuration	Lmax	CL _{max} ,	C _m curve	Figure
D ₁					2y/b = 0.658	•97	* 31.0	C _m 1	
D ₁			_	_	2y/b = 0.708	1.03	24.0		
D ₁					24/p = 0.408	•97	\$ 31.0		
D ₁					2y/b = 0.708	1.02	24.6		
D ₁					2y/b = 0.708	1.02	24.0		
D ₁					2y/b = 0.708	•98	21.0		
D ₁			7		29/6 = 0.658	1.03	23.0		
D ₁					2y/b = 0.658	1.03	23.0		

^{*}Highest angle of test

TABLE V.- Continued

$$R = 9 \times 10^6$$

Inlet	T.E. device	L.E. devi	се		Fence configuration	C.	a at	0. 0	74
	device	Туре	Span	Chord	Fence configuration	max	L _{max} ,	C _m curve	Figure
^D 1					2y/b = 0.658	•97	19.0	C _L .8 1.2 C _m .1	
D ₁					2y/b = 0.658	•97	* 31.0		
D ₁					h/t = 0.40 2y/b = 0.658	•96	19.0		
D ₁					2y/b = 0.658	1.03	22.0		
D ₁					2y/b = 0.658	1.01	20.0		
D1	-				2y/b = 0.658	•99	19.2		
D ₁					2y/b = 0.658	•97	31.0		
01			-		2y/b = 0.708 2y/b = 0.850	•97	\$ 31.0		

^{*}Highest angle of test

TABLE V.- Continued

$$R = 9 \times 10^6$$

Inle	T.E. device	L.E. dev	ice		Panas assistantian		a at		
	device	Туре	Span	Chord	Fence configuration	Lmax	C _{Lmax} ,	C _m curve	Figure
^D 1				_	2y/b = 0.658 2y/b = 0.708	1.01	21.0	0 .4 .8 1.2	
D ₁				_	2y/b = 0.658 2y/b = 0.708	1.01	23.0		
D ₁				_	2y/b = 0.658 2y/b = 0.708	1.00	23.0		
D ₁				_	2y/b = 0.658	•97	31.0		
D ₁				_	2y/b = 0.658 2y/b = 0.758	•98	20.4		
D ₁	Plain Flap 0.1399/2 to — 0.515b/2 0 = 400		_	_	2 y /b = 0.658	1.05	20.8	P	
D ₁	Plain Flap 0.139b/2 to 0.515b/2 0 = 40°				2y/b = 0.658	1.07	19.0		
D ₁	Plain Flap 0.139b/2 to 0.515b/2 0 _f = 40°				2y/b = 0.708	1.04	18.5		18
1	Plain Flap 0.139b/2 to 0.515b/2 0.515b/2				2y/b = 0.658	1.01	31.0		

*Highest angle of test

TABLE V.- Continued

$$\boxed{R = 9 \times 10^6}$$

Inlet	T.E.	L.S. devi	ce		Panas and day		a at		
iniet	device	Туре	Span	Chord	Fence configuration	Lmax	C _{Lmax} ,	C _m curve	Figure
^D 1		Chord-extension Normal leading-edge radius	0.608b/2 to 0.958b/2	0.117c		1.08	22.2	C _m 1-	
D ₁	_	Chord-extension Normal leading-edge radius	0.658b/2 to 0.958b/2	0.1170		1.08	22.5		19
^D 1		Chord-extension (drooped) Normal leading-edge radius	0.658b/2 to 0.958b/2	0.117c		1.08	31.0		
D ₁		Chord-extension Normal leading-edge radius	0.658b/2 to 0.908b/2	0.1170		1.07	24.0		
D ₁		Chord-extension Normal leading-edge radius	0.658b/2 to 0.858b/2	0.117c		1.07	24.0		
D ₁		Chord-extension Normal leading-edge radius	0.658b/2 to 0.808b/2	0.1170		1.06	23.0		1
D ₁	_	Chord-extension 2 × normal leading- edge radius	0.658b/2 to 0.958b/2	0.0590		1.08	26.0		
D1		Chord-extension 2 × normal leading- edge radius (inboard end faired)	0.658b/2 to 0.958b/2	0.0590		•97	31.0		

^{*}Highest angle of test

TABLE V.- Continued

$$\boxed{R = 9 \times 10^6}$$

Inlet	T.E. device					I.	a at		
		Type	Span	Chord	Fence configuration	Lmax	C _{Lmax} ,	C _m curve	Figure
D ₁		Chord-extension 2 × normal leading- edge radius	0.658b/2 to 0.808b/2	0.0590		1.06	24.2	O .4 .8 1.2	
D ₁		Chord-extension 2 × normal leading- edge radius	0.658b/2 to 0.758b/2	0.0590		1.04	25.0		
D ₁		Chord-extension 2 × normal leading- edge radius	0.658b/2 to 0.708b/2	0.0590		•98	21.0		
D ₁		Chord-extension 2 × normal leading- edge radius (outboard end faired)	0.658b/2 to 0.708b/2	0.059c		1.04	24.0		
D ₁		Chord-extension 2 × normal leading- edge radius	0.658b/2 to 0.958b/2	0.0290		1.01	21.0	P	
D ₁		Chord-extension 2 × normal leading- edge radius	0.658b/2 to 0.808b/2	0.029c		1.01	22.0		
D ₁		Chord-extension Sharp leading edge	0.608b/2 to 0.958b/2	0.059c		•99	* 31.0		
D ₁		Chord-extension Sharp leading edge	0.658b/2 to 0.958b/2	0.059e		•99	* 31.0		

^{*}Highest angle of test

TABLE V.- Continued

$$\boxed{R = 9 \times 10^6}$$

Inlet	T.E. device	L.E. dev	ice		Pence configuration	_	aat	
THIE	device	Туре	Span	Chord	Pence configuration	Lmax	CL _{max} ,	C _m curve Figure
D ₁		Chord-extension Sharp leading edge	0.708b/2 to 0.958b/2	0.0590		•98	* 31.0	o .4 .8 1.2 o .1 o .1 -2 3
D ₁		Chord-extension Sharp leading edge	0.758b/2 to 0.958b/2	0.0590		•97	* 31.0	
D ₁		Chord-extension Sharp leading edge	0.658b/2 to 0.808b/2	0.059e		•98	\$ 31.0	
D ₁		Chord-extension Sharp leading edge	0.558b/2 to 0.708b/2	0.0590		•97	31.0	
D ₁		Chord-extension Sharp leading edge	0.508b/2 to 0.658b/2	0.0590		•96	31.0	
D ₁		Chord-extension Sharp leading edge	0.458b/2 to 0.608b/2	0.0590		•96	31.0	
D ₁		Chord-extension Sharp leading edge	0.358b/2 to 0.508b/2	0.0590		•96	* 31.0	
D ₁		Chord-extension Sharp leading edge	0.308b/2 to 0.458b/2	0.059c		•97	31.0	

Highest angle of test

TABLE V.- Continued

$$\boxed{R = 9 \times 10^6}$$

nlet	T.E. device	L.E. de	vice		Fence configuration	c.	a at	C _m curve	Figur
.100	device	Туре	Span	Chord	2011 1541 401011	Lmax	C _{Lmax} ,	m out to	- Sul
P ₁		Chord extension Sharp leading edge	0.308b/2 to 0.508b/2	0.059c		•97	* 31.0	0 .4 ^C L.8 1.2	
D ₁	-	Chord extension Sharp leading edge (inboard end faired)	0.358b/2 to 0.508b/2	0.059c		•97	\$ 31.0		
D ₁		Chord extension 2 × normal leading- edge radius	0.658b/2 to 0.958b/2	0.1170		1.06	24.5		
D ₁		Chord extension 2 × normal leading- edge radius	0.658b/2 to 0.808b/2	0.1170		1.00	\$ 31.0		
1	Plain Flap 0.139b/2 to 0.515b/2 5 = 40°	radius	0.658b/2 to 0.958b/2	0.1170		1.10	18.0		19
D ₁	Plain Flap 0.139b/2 to 0.515b/2 5 _f = 20°	radius	0.658b/2 to 0.958b/2	0.1170		1.09	20.8		
D ₁	Plain Flap 0.139b/2 to 0.515b/2 0.515b/2	radius	0.683b/2 to 0.958b/2	0.1170		1.08	19•0		
D ₁	Plain Flap 0.139b/2 to 0.515b/2 5 _f = 40°	Normal leading-edge radius	0.658b/2 to 0.808b/2	0.1170		1.05	17.0		

^{*}Highest angle of test

TABLE V.- Continued

$$\boxed{R = 9 \times 10^6}$$

Inlet	T.E.	L.E. devi	ce		Fence configuration		a at	Country	Figure
TITE	device	Туре	Span	Chord	. Jaco Configuration	Lmax	C _{Lmax} ,	C _m curve	- Igure
D ₁	Plain Flap 0.139b/2 to 0.515b/2 8 = 40°	Chord-extension 2 × normal leading- edge radius	0.658b/2 to 0.808b/2	0.0590		1.06	19.0	C _m 1	
D ₁	Plain Flap 0.139b/2 to 0.515b/2 \$f = 409	Chord-extension Sharp leading edge	0.358b/2 to 0.508b/2	0.0590		1.02	31. 0		
D ₁		Leading-edge modification 2 × normal leading- edge radius	0.398b/2 to 0.958b/2			•99	* 31.0		
D ₁		Leading-edge modification 2 × normal leading- edge radius	0.458b/2 to 0.958b/2			•99	31.0		
D ₁		Leading-edge modification 2 × normal leading-edge radius	0.558b/2 to 0.958b/2	1		-97	31.0		
D ₁		Leading-edge modification 2 × normal leading- edge radius	0.608b/2 to 0.958b/2			•97	* 7 31.0		
D ₁		Leading-edge modification 2 × normal leading- edge radius	0.633b/2 to 0.958b/2	-		•97	7 31.0		
D ₁		Leading-edge modification 2 × normal leading- edge radius	0.652b/2 to 0.958b/2			•91	7 22.0		
D ₁		Leading-edge modification 2 × normal leading-edge radius (inboard end faired)	0.652b/2 to 0.958b/2			•9	7 31.0		
D ₁		Leading-edge modification 2 × normal leading- edge radius	0.683b/2 to 0.958b/2			•9	7 31.0		

^{*}Highest angle of test

TABLE V.- Continued

$$\boxed{R = 9 \times 10^6}$$

Inlet	T.E. device	L.S. dev	rice		Pence configuration		a at		
	device	Туре	Span	Chord	Fence configuration	Lmax	C _{Lmax} ,	C _m curve	Figur
D ₁		Leading-edge modification 2 × normal leading-edge radius	0.708b/2 to 0.958b/2			•97	31.0	C _m 1	
D ₁		Leading-edge modification 2 × normal leading- edge radius	0.652b/2 to 0.802b/2			•97	31.0		
D ₁		Leading-edge modification 2 × normal leading-edge radius (upper surface)	0.652b/2 to 0.958b/2		-	•98	26.0		
D ₁		Leading-edge modification 2 × normal leading- edge radius	0.652b/2 to 0.958b/2		2y/b = 0.850	•99	31.0		
D ₁		Leading-edge modification 2 × normal leading- edge radius	0.652b/2 to 0.958b/2	_	2y/b = 0.708	1.01	31.0		
21		Leading-edge modification 2 × normal leading- edge radius	0.652b/2 to 0.958b/2		2y/b = 0.658	1.03	25.0		
01		Leading-edge modification 2 × normal leading-edge radius (inboard end faired)	0.652b/2 to 0.958b/2		2y/b = 0.608	1.01	* 31.0		
-		Leading-edge modification 2 × normal leading- edge radius	0.652b/2 to - 0.958b/2		2y/b = 0.482 2y/b = 0.652	•98	23.0		18

^{*}Highest angle of test

TABLE V.- Continued

$$\boxed{R = 9 \times 10^6}$$

-101	T.E. device	L.S. dev	ice		Fence configuration	C.	a at	C _m curve	Figure
inlet	device	Туре	Span	Chord		Lmax	C _{Lmax} ,		-0
	Plain Flap 0.139b/2 to 0.155b/2 8 _f = 40°	Leading-edge modification 2 × normal leading- edge radius	0.652b/2 to 0.958b/2		2y/b = 0.658	1.03	25.0	0 .4 L.8 1.2	
D ₀ + Sharp Side Body						1.07	\$ 31.0		13
D _O			_			1.04	31.0		13
D ₀					2 y /b = 0.658	1.11	23.1	b.	
D ₀			-		2y/b = 0.758	1.05	31.0		
D _O			_	-	2y/b = 0.558 2y/b = 0.658	1.0	31.0		
D ₀	_				2y/b = 0.608 2y/b = 0.758	1.07	7 28.0		
Do					2y/b = 0.658	1.00	\$ 31.0		
Do					2y/b = 0.758 2y/b = 0.900		4 31.0		

^{*}Highest angle of test

TABLE V.- Continued

$$\boxed{R = 9 \times 10^6}$$

Inle	T.E. device	L.E. dev	lce		Banca and A		a at		
inte	device	Туре	Span	Chord	Pence configuration	Lmax	CL _{max} ,	C _m curve	Figure
D ₀			_		2y/b = 0.708 2y/b = 0.850	1.06	24.0	0 .4 .8 1.2 0	
Do					2y/b = 0.708 2y/b = 0.850	1.04	# 31.0		
Do		4		_	2y/b = 0.708 2y/b = 0.850	1.04	* 31.0		
Do					2y/b = 0.708 2y/b = 0.850	1.04	* 31.0		
Do					2y/b = 0.558 2y/b = 0.708 2y/b = 0.850	1.05	* 31.0		
D _O	Plain Flap 0.139b/2 to 0.155b/2 0 = 40°				2y/b = 0.708	1.04	* 31.0		
D _O		Chord-extension Normal leading-edge radius	0.608b/2 to 0.958b/2	0.117c		1.08	* 31.0		
Do		Chord-extension Normal leading-edge radius	0.658b/2 to 0.958b/2	0.1170		1.12	22.2		
Do		Chord-extension Normal leading-edge radius	0.683b/2 to 0.958b/2	0.1170		1.16	25.5		

"Highest angle of test

TABLE V.- Continued

$$\boxed{R = 9 \times 10^6}$$

Inlet	T.E.	L.E. devi	се				a at		
TITE	device	Туре	Span	Chord	Fence configuration	CLmax	CL _{max} ,	C _m curve	Figure
D ₀		Chord-extension Normal leading-edge radius	0.708b/2 to 0.958b/2	0.1170		1.12	25.0	O .li .8 1.2 .l	19
D ₀	_	Chord-extension Normal leading-edge radius	0.758b/2 to 0.958b/2	0.1170		1.10	* 31.0		
D _O	_	Chord-extension Normal leading-edge radius	0.708b/2 to 0.858b/2	0.1170		1.09	* 31.0		
D ₀	_	Chord-extension Normal leading-edge radius	0.708b/2 to 0.958b/2	0.0590		1.12	24.0		
D _O		Chord-extension Normal leading-edge radius	0.708b/2 to 0.858b/2	0.0590		1.09	24.0	P	
Do	_	Chord-extension 2 × normal leading- edge radius	0.708b/2 to 0.958b/2	0.1170		1.17	26.2		
D _O		Chord-extension 2 × normal leading- edge radius	0.708b/2 to 0.858b/2	0.1170		1.07	27.4		
Do		Chord-extension 2 × normal leading- edge radius	0.708b/2 to 0.958b/2	0.0590		1.17	25.1		
Do		Chord-extension 2 × normal leading- edge radius	0.708b/2 to 0.858b/2	0.059c		1.12	24.1		
D _O	Plain Flap 0.139b/2 to 0.515b/2 5 _f = 400	Chord-extension Normal leading-edge radius	0.658b/2 to 0.958b/2	0.1170		1.15	22.0		

^{*}Highest angle of test

TABLE V.- Continued

$$\boxed{R = 9 \times 10^6}$$

Inlet	T.E.	L.E. dev	ice		Bence confirmation		a at		
	device	Туре	Span	Chord	Fence configuration	Lmax	C _{Lmax} ,	C _m curve	Figure
D _O	Plain Flap 0.139b/2 to 0.515b/2 0 = 40°	Chord-extension Normal leading-edge radius	0.708b/2 to 0.958b/2	0.117c		1.14	20.8	C _L 0 .4 .8 1.2 0 .4 .8 1.22	19
0	Plain Flap D.139b/2 to	Chord-extension Normal leading-edge radius	0.683b/2 to 0.958b/2	0.1170		1.15	22.0		
	Plain Flap 0.139b/2 to 0.515b/2 bf = 40°	Chord-extension Normal leading-edge radius	0.708b/2 to 0.858b/2	0.1170		1.14	22.1		
D ₀		Leading-edge modification 2 × normal leading- edge radius	0.652b/2 to 0.958b/2			1.05	# 31.0		
D _O		Leading-edge modification 2 × normal leading- edge radius	0.652b/2 to 0.958b/2		2y/b = 0.482	1.12	23.1	b.	
D ₀		Leading-edge modification 2 × normal leading- edge radius	0.708b/2 to 0.958b/2		2y/b = 0.708 2y/b = 0.850	1.04	\$ 31.0		
D _O		Leading-edge modification 2 × normal leading-edge radius	0.652b/2 to 0.958b/2		2y/b = 0.482 2y/b = 0.652	1.15	25.2		21
	Plain Flap 0.139b/2 to 0.515b/2 8f = 409	Leading-edge modification 2 × normal leading- edge radius	0.708b/2 to 0.958b/2		2y/b = 0.708 2y/b = 0.850	1.10	# 31.0		
D _O	Plain Flap 0.139b/2 to 0.515b/2 0f = 40°	Leading-edge modification 2 × normal leading-edge radius	0.652b/2 to 0.958b/2		2y/b = 0.482 2y/b = 0.652	1.10	* 31.0		22

TABLE V.- Concluded

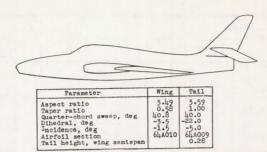
$$\begin{bmatrix} R = 9 \times 10^6 \end{bmatrix}$$

Inlat	T.E. device	L.S. dev	ice		Panas and		a at		
miet	device	Туре	Span	Chord	Pence configuration	Lmax	CL _{max} ,	C _m curve	Figure
Do	Plain Flap 0.139b/2 to 0.515b/2 0_f = 40°	Leading-edge modification 2 × normal leading-edge radius	0.652b/2 to 0.958b/2		2y/b = 0.4182 2y/b = 0.652	1.10	\$ 31.0	C _m 1	
D ₀ 1		-				1.04	\$1.0		13
D ₀ 1	_		-		2y/b = 0.658	1.09	22.0	1	
D01					2y/b = 0.708	1.11	24.1		14
D ₀ 1	_				2y/b = 0.758	1.09	26.0		
D ₀₂		-				1.04	31.0		13
D02	_				2y/b = 0.708	1.12	24.1		14
D ₀₂	_				2y/b = 0.608 2y/b = 0.758	1.08	26.5		
D02			-		2y/b = 0.658 2y/b = 0.850	1.03	* 31.0		
D ₀₂			_		2y/b = 0.708 2y/b = 0.850	1.04	\$ 31.0		14

^{*}Highest angle of test

TABLE VI

 $\boxed{R = 9 \times 106}$



			Tail h	eight, w	ring semispan	0.28					
Inlet	T.E.	L.E. devic	0		Fence configuration	c _L	a at	C _m curve	Figure		
	device	Туре	Span	Chord				CL _{max} ,			
	_			-		•95	31.0	O .4 .8 1.2	17		
D ₃	_					•95	* 31.0		17		
D ₂				-		•97	* 31:0		17		
D ₁	_			-		-97	* 31.0		17		
D ₁	_	Leading-edge modification 2 × normal leading- edge radius	0.652b/2 to 0.958b/2			•97	# 31.0				
D ₁		Leading-edge modification 2 × normal leading- edge radius	0.652b/3 to 0.958b/3		2y/b = 0.850	•99	31.0				

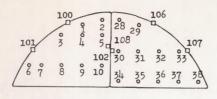
^{*}Highest angle of test

TABLE VI.- Concluded

$$\boxed{R = 9 \times 10^6}$$

inlet	T.E.	L.E. device			Panas confirmation		a at		
IIIe	device	Type Span Chord	Fence configuration	Lmax	CL _{max} ,	C _m curve	Figure		
D ₁		Leading-edge modification 2 × normal leading-edge radius	0.652b/2 to 0.958b/2		2y/b = 0.608 2y/b = 0.850	•99	* 31.0	C _L .8 1.2	
D _O	_					1.06	* 31.0		17
D _O		Leading-edge modification 2 × normal leading- edge radius	0.652b/2 to 0.958b/2		2y/b = 0.482 2y/b = 0.652	1.17	25.2		21
D _O	Plain Flap 0.139b/2 to 0.515b/2 $\delta_{\mathbf{f}} = 409$	0	0.652b/2 to 0.958b/2		2y/b = 0.482 2y/b = 0.652	1.17	24.0		22

^{*}Highest angle of test



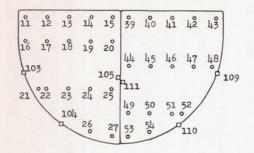


TABLE VII PRESSURE RECOVERY MEASUREMENTS AT THE COMPRESSOR FACE LOCATION FOR VARIOUS BOUNDARY-LAYER DIVERTER CONFIGURATIONS, INLET D_1 .

	Diverter Bloo	k	Splitter	Plate No. 1	Splitter	Plate No. 2
Orifice Number	H ₁ - P _o	$\frac{P_l - P_o}{q_o}$	H ₁ - P _o	$\frac{P_l - P_o}{q_o}$	H ₁ - P ₀	P _l - P _o
			$\alpha = 0^{\circ}$			
12345678910	0.479 -5737 -7658 -559 -418 -9560 -842		0.578 .587 .827 .860 .567 .357 .981 .993 .994 .896		0.547 .579 .823 .509 .582 .530 .985 .995 .875	
100 101 102		0.064 .145 .238		0.064 .140 .068		0.065 •137 •203
11 12 13 15 16 17 18 190 21 223 24 256 27	•996 •9995 •995 •972 •997 •997 •992 •978 •992 •992 •992 •963 •7750 •603		996 996 9987 9987 9988 9988 9988 9988 99		995 996 996 9988 988 9988 9912 9912 9993 988 888 888 740	
103 104 105		.002 .247 .460		•039 •270 •484		•045 •282 •495
28 29 33 33 33 35 35 37 37 37 37 37 37 37 37 37 37 37 37 37	.4877 .6377 .86377 .9882 .4548 .985 .600 126		.639 .597 .660 .970 .984 .455 .986 .671 -122 -107		.649 .614 .649 .972 .994 .446 .992 .682 129	

TABLE VII.- Continued $\label{thm:compressor} \mbox{ pressure recovery measurements at the compressor face location for various boundary-layer diverter configurations, inlet <math display="inline">\mbox{ d}_1. \mbox{ exit full open }$

	Diverter Bloo	k	Splitter 1	Plate No. 1	Splitter 1	Plate No. 2
rifice umber	H ₁ - P ₀	P _l - P _o	H1 - Po	Pl - Po	H ₁ - P ₀	$\frac{P_l - P_o}{q_o}$
106 107 108		0.266 043 316		0.275 037 037		0.275 051 332
39012345678901234	0 9845 9845 9887 9759 - 3360 9832 9854 9854 9854 98557		0.943 .983 .985 .981 .975 .765 -283 .799 .980 .608 .818 .977 .982 .625 .799		0.959 .993 .991 .991 .981 -274 -274 .995 .995 .650 .800 .981	
109 110 111		0 .296 .490		•024 •323 •509		•026 •330 •518
			a = 10.6°		A.	
1 2 3 4 5 6 7 8 9 10 100 101 102	0.677 .676 .832 .988 .838 .295 .972 .986 .986	0.070 .123 .208	0.666 .706 .835 .993 .883 .295 .978 .992 .993	0.080 .141 .104	0.664 .699 .825 .990 .880 .269 .981 .984	0.063 .122 .153
11 12 13 14 15 16 17 19 19 20 21 22 22 25 27	.990 .993 .987 .989 .989 .990 .980 .969 .975 .975 .975 .677 .560 .645 .512		.992 .993 .990 .977 .970 .989 .993 .964 .891 .896 .986 .986 .986 .985 .780 .604 .621		•994 •993 •995 •986 •980 •986 •986 •986 •986 •987 •989 •808 •535 •718 •613	
103 104 105		•035 •258 •396		.087 .275 .449		.033 .260 .410

	Diverter Block		Splitter P	late No. 1	Splitter	Plate No. 2
Orifice Number	$\frac{H_1 - P_0}{q_0}$	Pl-Po	H ₁ - P ₀	P _l - P _o	$\frac{H_1 - P_0}{q_0}$	$\frac{P_l - P_o}{q_o}$
28 299 301 333 334 337 337 337 337 337 337	0.751 .729 .985 .987 .984 .422 .852 .986 .662 -139		0.698 .723 .981 .983 .982 .424 .817 .983 .672 -136		0.707 .735 .988 .994 .994 .447 .894 .998 .679 150	700 200
106 107 108		0.249 071 318		0.251 068 307		0.063 .122 .153
34444444445555555555555555555555555555	986 9889 9889 9887 9880 8239 -6072 9386 6405 -5757 -5437		974 984 9884 9873 7791 - 1793 9779 - 4982 - 4982 - 8591 - 612		•978 •995 •996 •996 •992 •803 •196 •677 •975 •998 •614 •605 •686 •832 •558 •577	
109 110 111		.048 .321 .424		•052 •339 •457		•051 •328 •453
			α = 21.0°		V 680	
12 34 56 78 9 10 100 1001	0.136 .147 .127 .134 .145 .191 .162 .164 .163	021 .120	0.157 .145 .145 .151 .162 .232 .186 .196 .189	011	0.145 .154 .155 .140 .155 .254 .192 .194 .186	010 .128
102 112 137 144 155 16 177 188 190 211 223 244 226 27	.4325 .2313 .2313 .2370 .5306 .22670 .5306 .2265 .2450 .5540	041	5280 454591 423514597 425582 556632 56632 56632	-133	• 519 • 391 • 249 • 245 • 366 • 546 • 546 • 244 • 275 • 450 • 579 • 648 • 548 • 548 • 413	083

TABLE VII.- Concluded

PRESSURE RECOVERY MEASUREMENTS AT THE COMPRESSOR FACE LOCATION FOR VARIOUS
BOUNDARY-LAYER DIVERTER CONFIGURATIONS, INLET D1. EXIT FULL OPEN

	Diverter Block		Splitter P	late No. 1	Splitter	Plate No. 2
Orifice Number	H _i - P _o	$\frac{P_l - P_o}{q_o}$	H ₁ - P ₀	$\frac{P_1 - P_0}{q_0}$	$\frac{H_1 - P_0}{q_0}$	$\frac{P_l - P_o}{q_o}$
103 104 105		-0.072 .061 .241		-0.071 .074 .282		-0.074 .066 .262
28 29 31 23 33 33 35 37 37 37 37 37 37 37	0.187 .160 .193 .181 .178 .192 .205 .231 .266 .220		0.176 .149 .179 .166 .174 .218 .206 .235 .308 .263		0.178 .149 .173 .162 .163 .191 .198 .226 .272 .246 .159	
106 107 108		•142 •123 ••287		•143 •134 ••299		•135 •130 ••383
34445678901234 9012345678901234	.390 .2854 .3407 .3740 .1747 .5715 .609 .4809		•393 •270 •274 •405 •547 •586 •067 •192 •1448 •639 •573 •706 •696 •645 •523 •447		• • • • • • • • • • • • • • • • • • •	
109 110 111		071 .119 .261		093 .122 .283		083 .112 .272

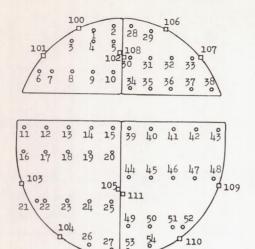


TABLE VIII $\begin{tabular}{ll} \textbf{PRESSURE RECOVERY MEASUREMENTS AT THE COMPRESSOR} \\ \textbf{FACE LOCATION FOR INLET} & D_2 & \textbf{WITH ORIGINAL} \\ \textbf{BOUNDARY-LAYER DIVERTER BLOCK.} \\ \textbf{EXIT FULL OPEN} \\ \end{tabular}$

	$\alpha = 0^{\circ}$			10.6°		20.9°
Orifice Number	$\frac{H_1 - P_0}{q_0}$	$\frac{\overline{P}_{l} - \overline{P}_{0}}{q_{0}}$	$\frac{H_1 - P_0}{q_0}$	$\frac{P_l - P_0}{q_0}$	$\frac{H_1 - P_0}{q_0}$	$\frac{P_{l} - \overline{P}_{o}}{q_{o}}$
1 2 3 4 5 6 7 8 9	0.509 .607 .794 .726 .546 .776 .987 .991 .991		0.709 .710 .817 .995 .873 .606 .992 .991		0.169 .178 .166 .165 .171 .181 .174 .169 .168	
100 101 102		.102 .369		0.101		0.038
11 12 13 14 15 16 17 18 19 21 22 21 22 21 26 27			 •997 •993 •993 •992 •000 •993 •970 •991 •991 •991 •843 •570 •637 •608		-1-6 -1-76 -2955 -2955 -2952 -2918 -29918 -198 -198 -198 -198 -198 -198 -198	
103 104 105		.032 .338 .492		.020 .321 .414		136 .079 .268
28 29 30 30 30 30 30 30 30 30 30 30 30 30 30	• 549 • 554 • 677 • 976 • 984 • • 987 • 717 • 108		.845 .710 .976 .981 .979 .887 .981 .714		.183 .165 .182 .160 .162 .194 .214 .214	

TABLE VIII .- Concluded

PRESSURE RECOVERY MEASUREMENTS AT THE COMPRESSOR FACE LOCATION FOR INLET D_2 WITH ORIGINAL BOUNDARY-LAYER DIVERTER BLOCK. EXIT FULL OPEN

Parts are	$\alpha = 0^{\circ}$			= 10.6°	α	= 20.9°
Orifice Number	H _i - P _o	P _l - P _o	H _i - P _o	$\frac{P_{l} - P_{o}}{q_{o}}$	H _i - P _o	$\frac{P_l - P_0}{q_0}$
106 107 108		0.290 .099 .426		0.244 .101 .499		0.163 .046 .169
34 41 44 44 44 44 45 55 55 55 55	0.950 .987 .986 .986 .272 .991 .969 .620 .743 .982 .631 .811		0.971 .975 .982 .980 .791 .740 .212 .953 .964 .572 .562 .723 .807 .508 .571		0.359 .262 .288 .471 	
109 110 111		.123		.119 .440		101

NACA RM L54B17

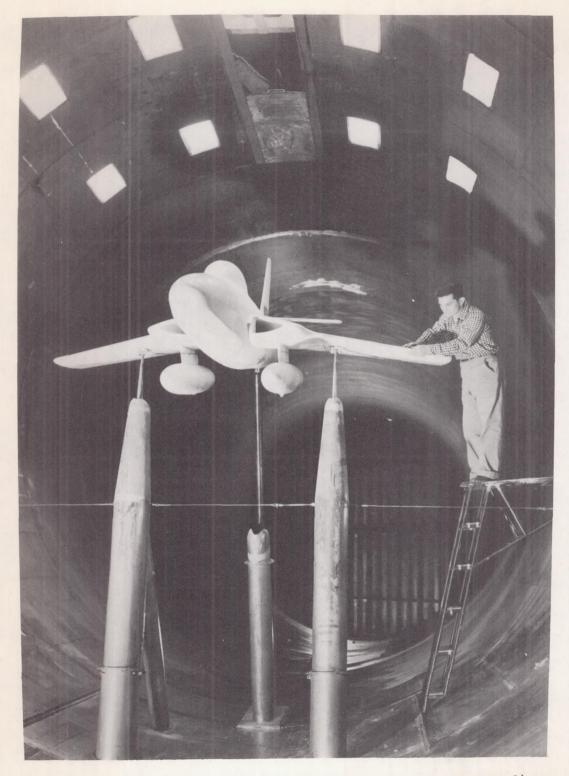


Figure 1.- The model installed in the Langley 19-foot pressure tunnel.

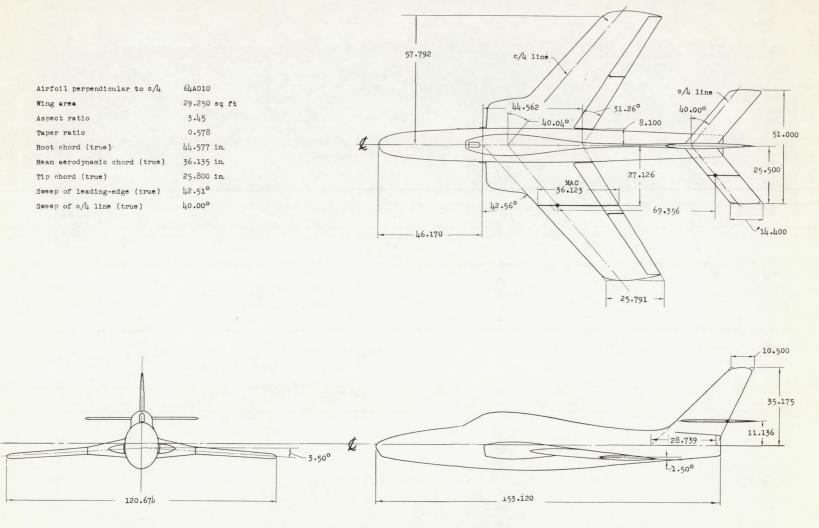


Figure 2.- Three-view drawing of the model. All dimensions are in inches.

N

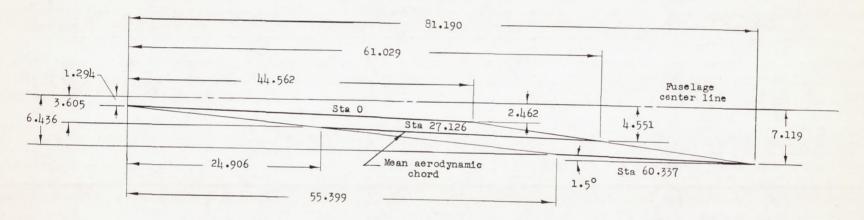


Figure 3.- Wing rigging diagram of the model. All dimensions are in inches.

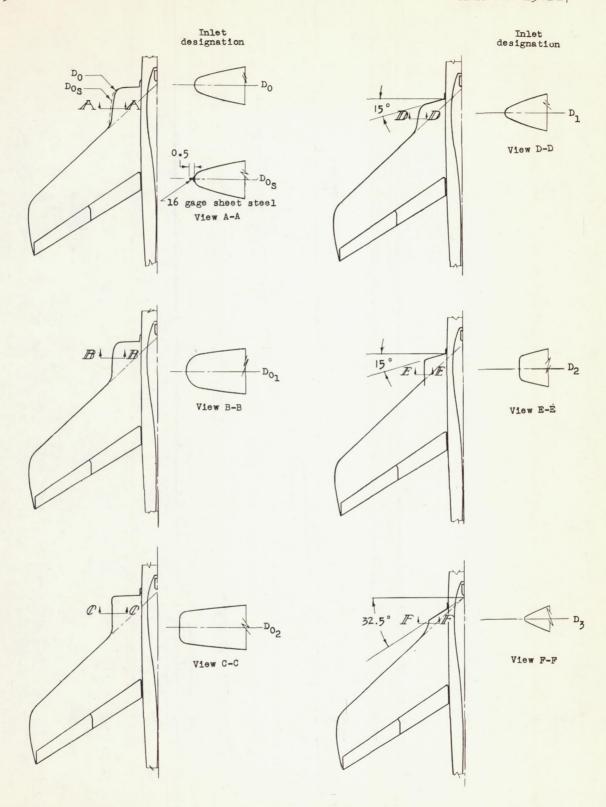


Figure 4.- Details of inlet plan forms and contours. All dimensions are in inches.

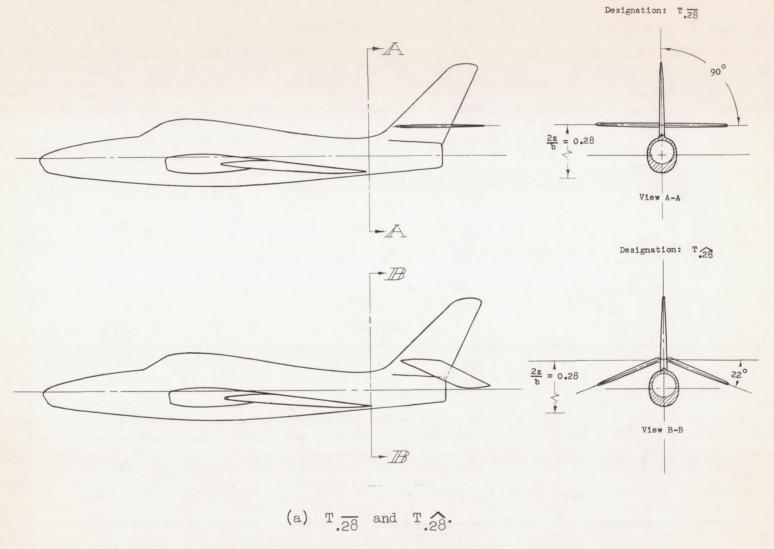
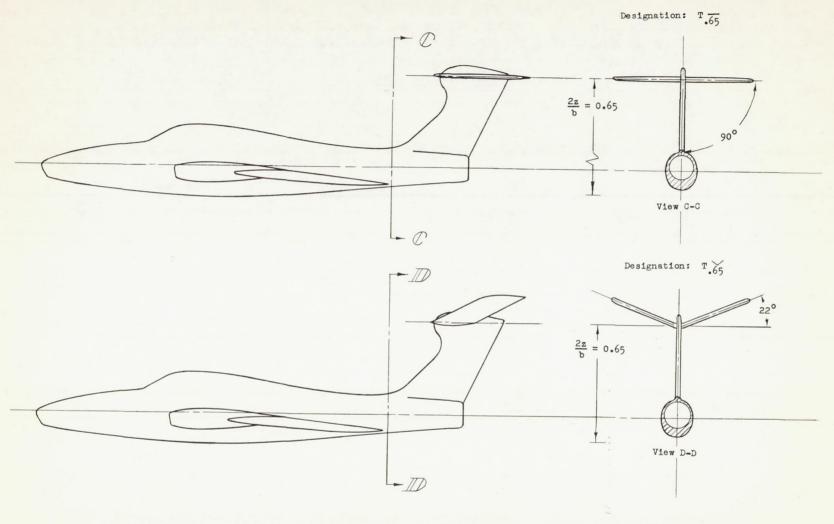


Figure 5.- Details of the various horizontal tail arrangements. All dimensions are in inches.



(b) T.65 and T.65.

Figure 5.- Concluded.

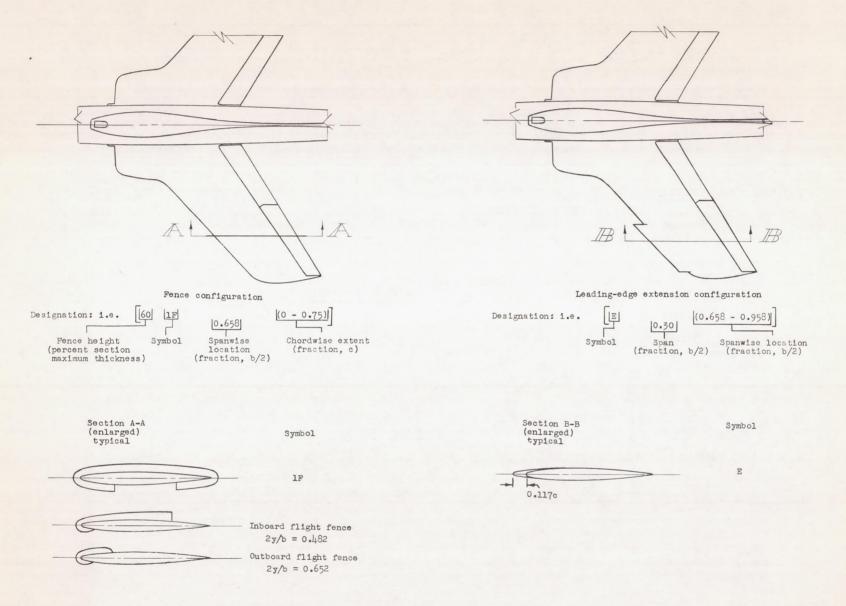
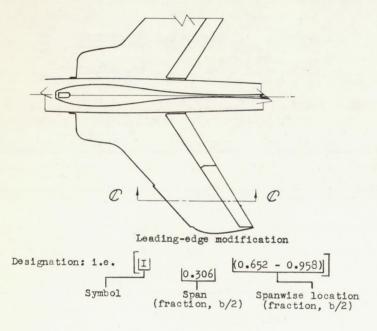
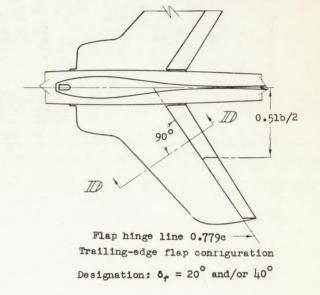
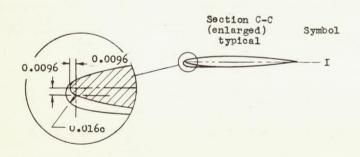


Figure 6.- Details of high-lift and stall-control devices.







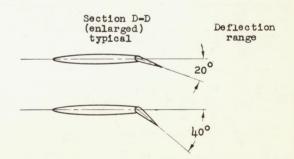
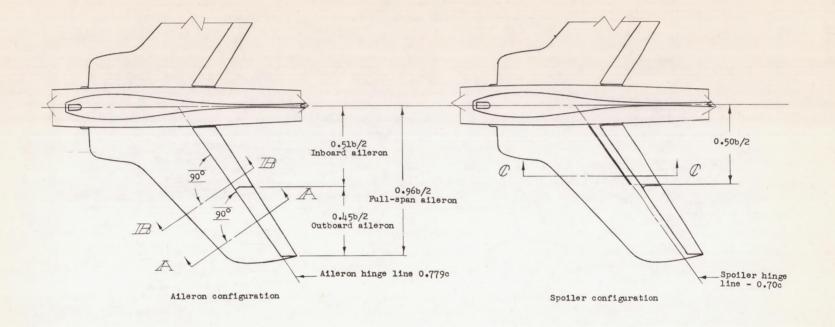


Figure 7.- Details of leading-edge modification and trailing-edge flaps.



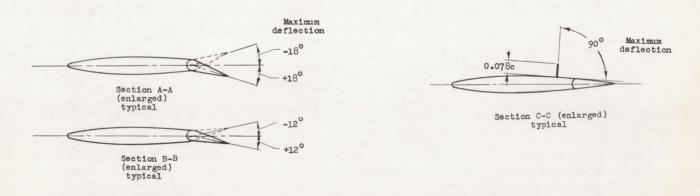


Figure 8.- Details of the various lateral-control devices. All dimensions are in inches.

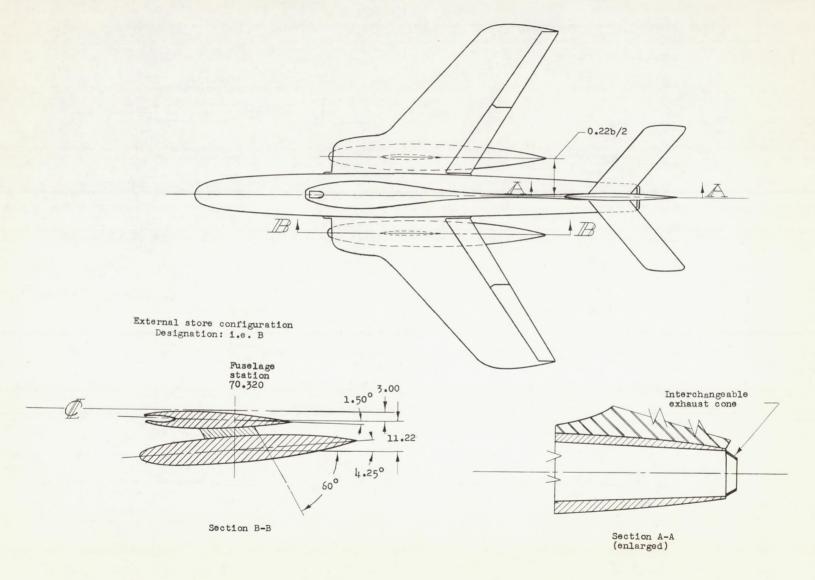


Figure 9.- Details of external store and exhaust cone installation. All dimensions are in inches.

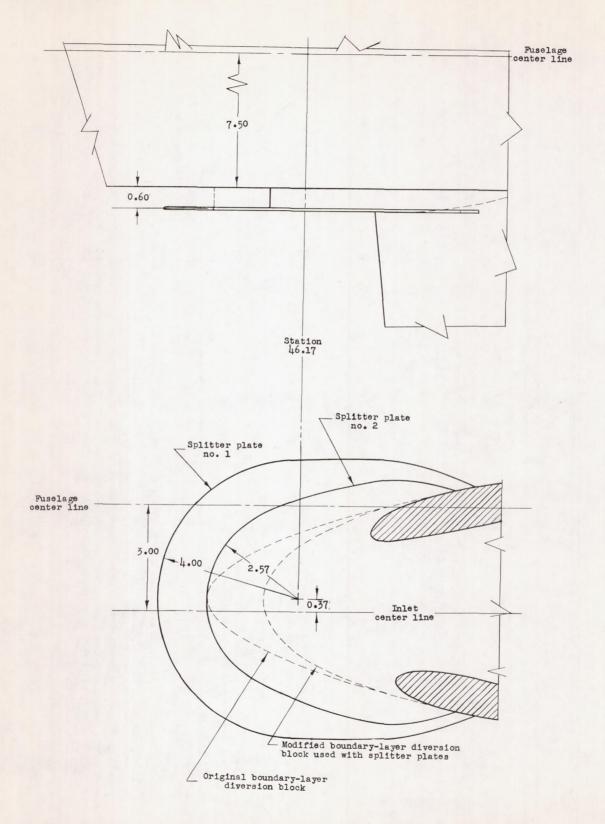


Figure 10.- Details of inlet boundary-layer diverters. All dimensions are in inches.

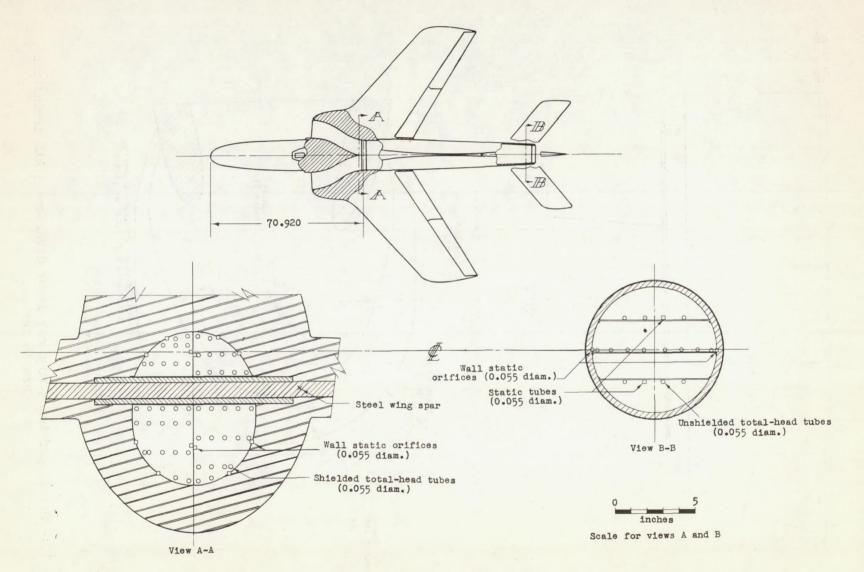
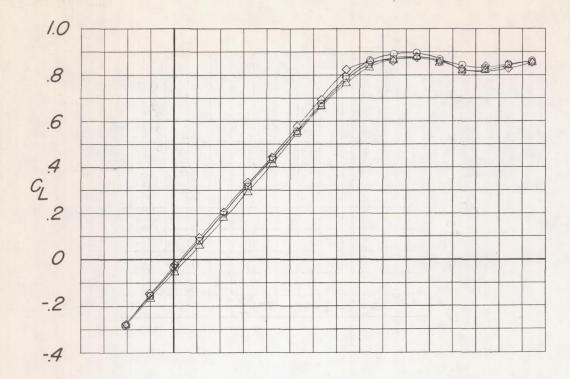


Figure 11.- Details of pressure rake installations. All dimensions are in inches.



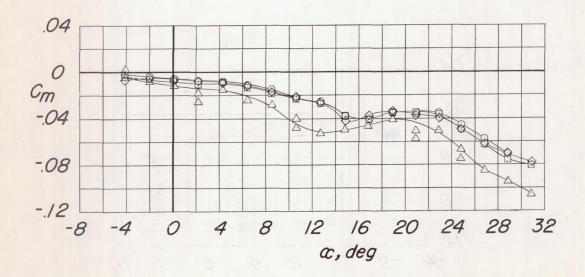
R

△ 2.2 × 10 6

□ 5.0

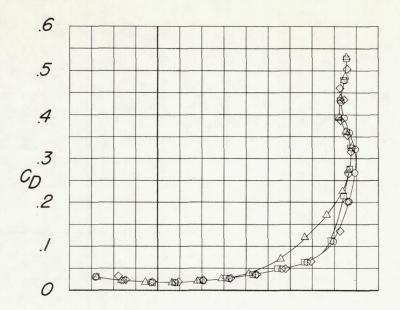
○ 9.0

◇ 11.0



(a) $C_{\rm L}$ and $C_{\rm m}$ against α .

Figure 12.- Effect of Reynolds number on the wing-fuselage-vertical-tail combination.



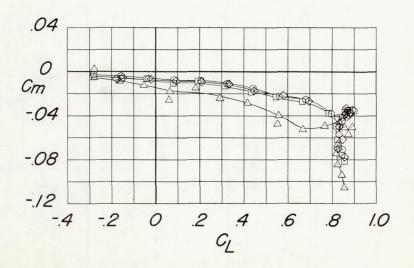
R

△ 2.2 × 10 6

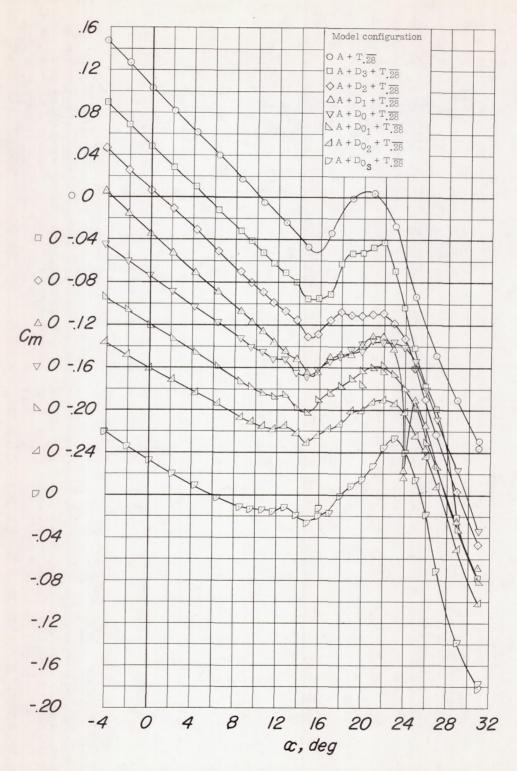
□ 5.0

○ 9.0

◇ 11.0

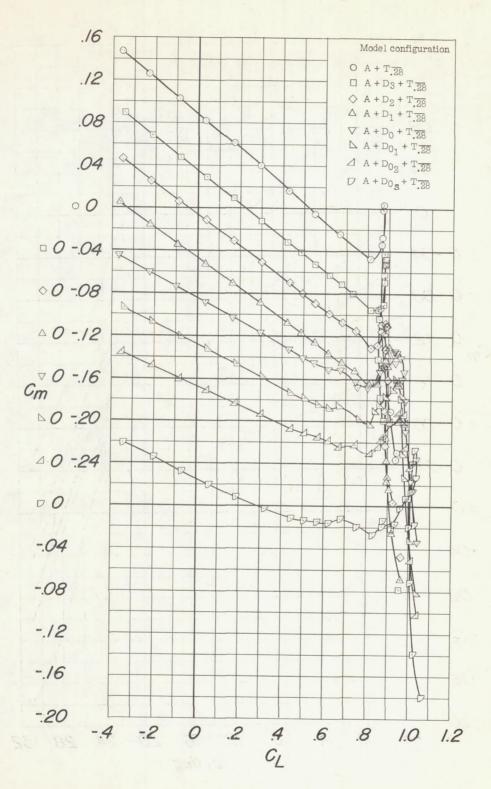


(b) C_{D} and C_{m} against $C_{\mathrm{L}}.$ Figure 12.- Concluded.



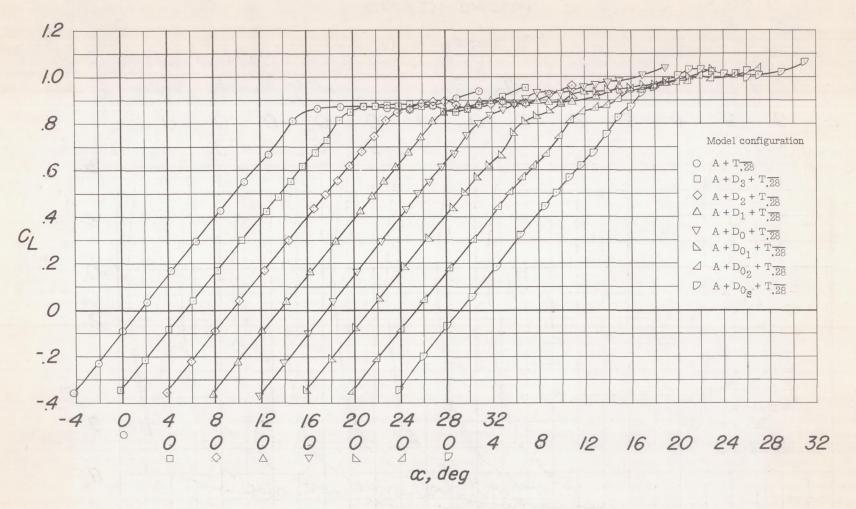
(a) C_m against α .

Figure 13.- The longitudinal characteristics of the model equipped with various inlets.



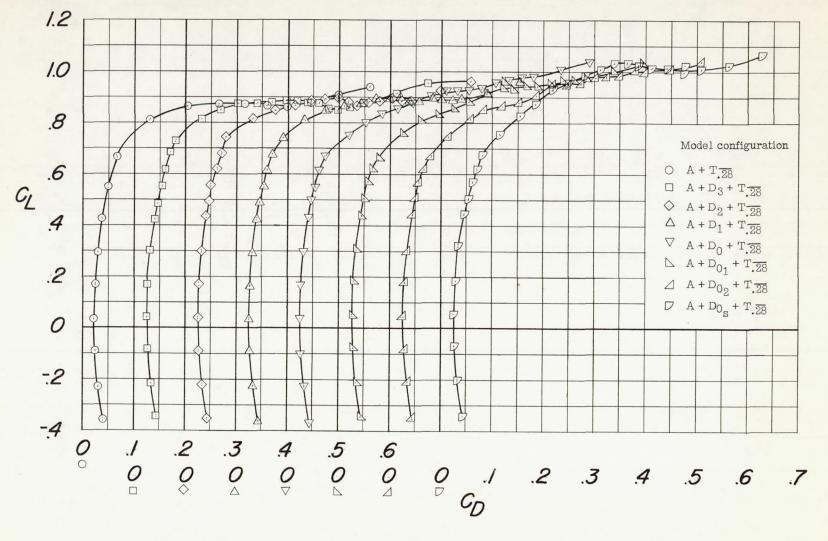
(b) $C_{\rm m}$ against $C_{\rm L}$.

Figure 13.- Continued.



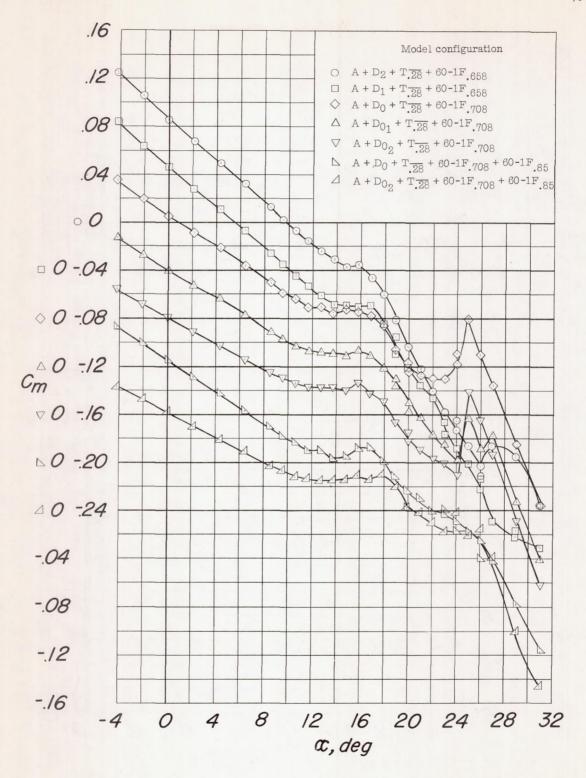
(c) C_L against α .

Figure 13.- Continued.



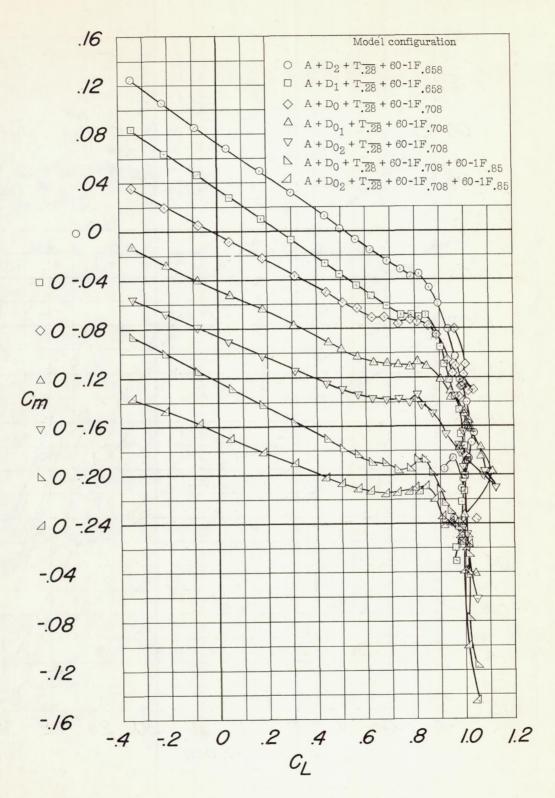
(d) C_L against C_D.

Figure 13.- Concluded.

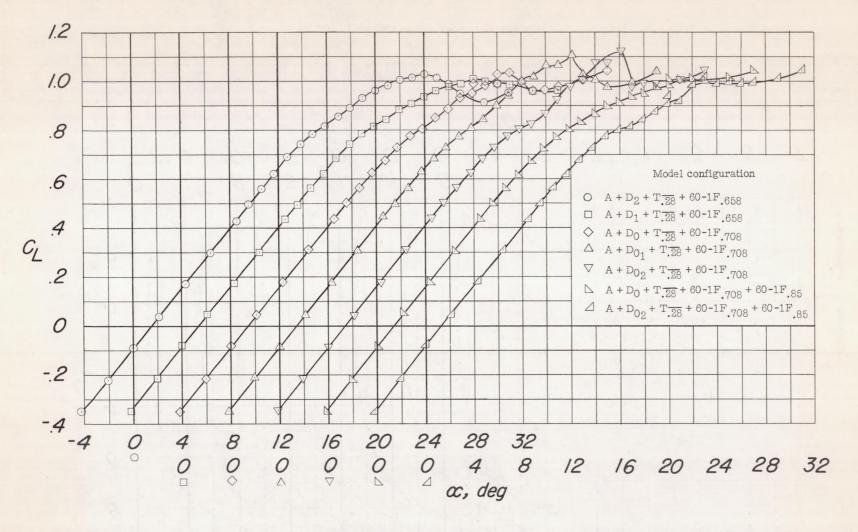


(a) C_m against α .

Figure 14.- The longitudinal characteristics of the model equipped with various inlets and wing fences.

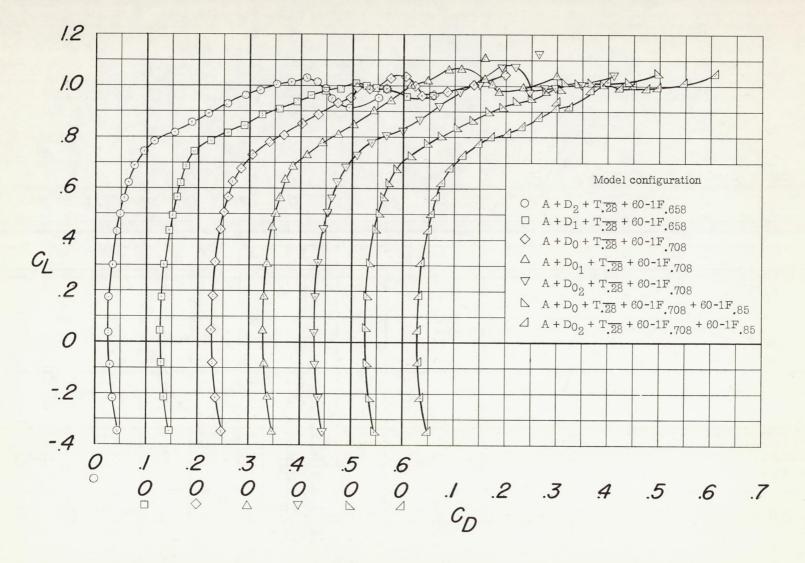


(b) $C_{\rm m}$ against $C_{\rm L}$.



(c) C_L against α .

Figure 14.- Continued.



(d) C_{L} against C_{D} .

Figure 14.- Concluded.

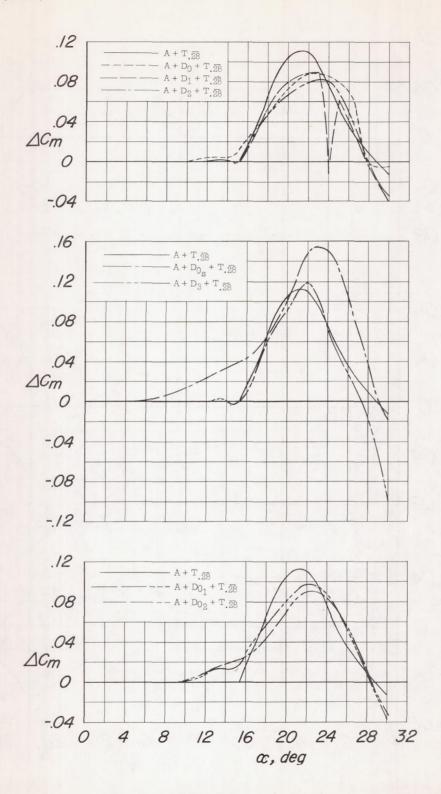
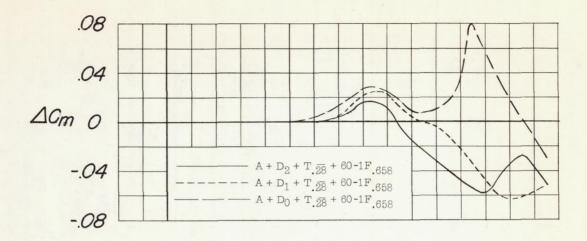
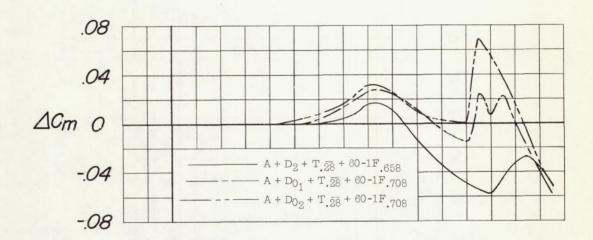


Figure 15.- The deviation with angle of attack of the pitching-moment coefficient from $\left(dC_m/d\alpha\right)_{\alpha=0}$ for the model equipped with the production tail and various inlets.





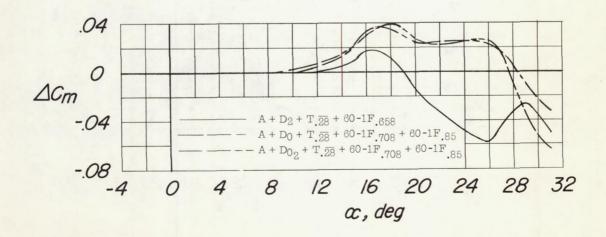
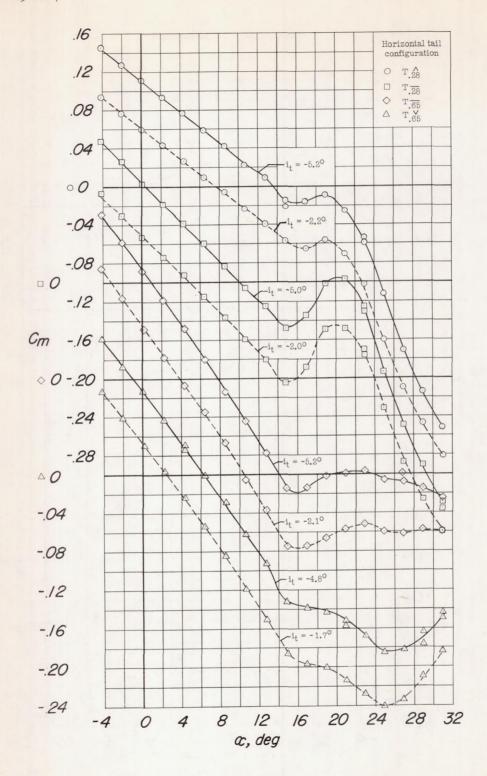
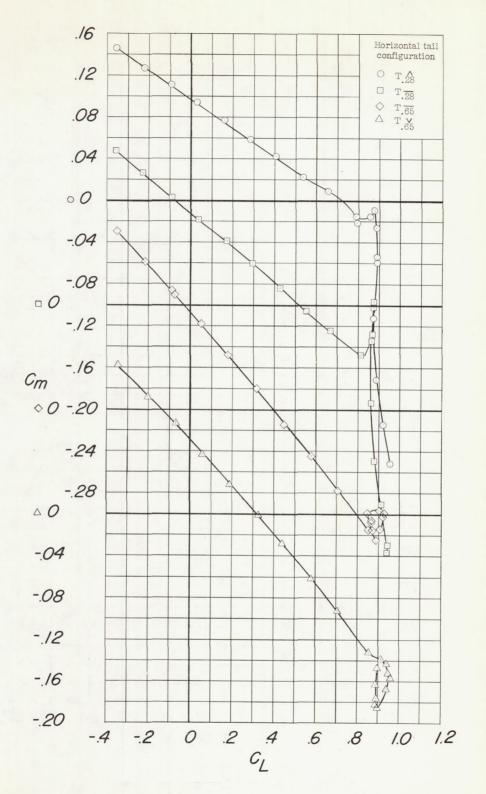


Figure 16.- The deviation with angle of attack of the pitching-moment coefficient from $\left(\text{dC}_m/\text{d}\alpha\right)_{\alpha=0}$ for the model equipped with the production tail and with various inlets and wing fences.

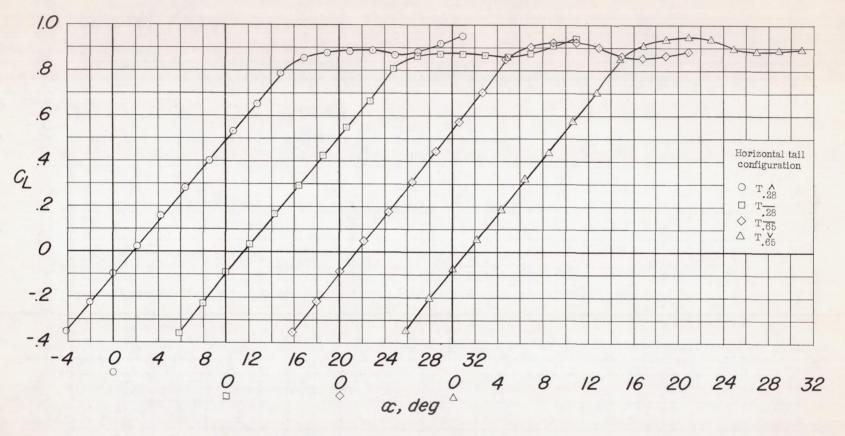


(a) Inlets off, C_{m} against α .

Figure 17.- Effect of horizontal-tail configuration on the longitudinal characteristics of the model equipped with various inlets.

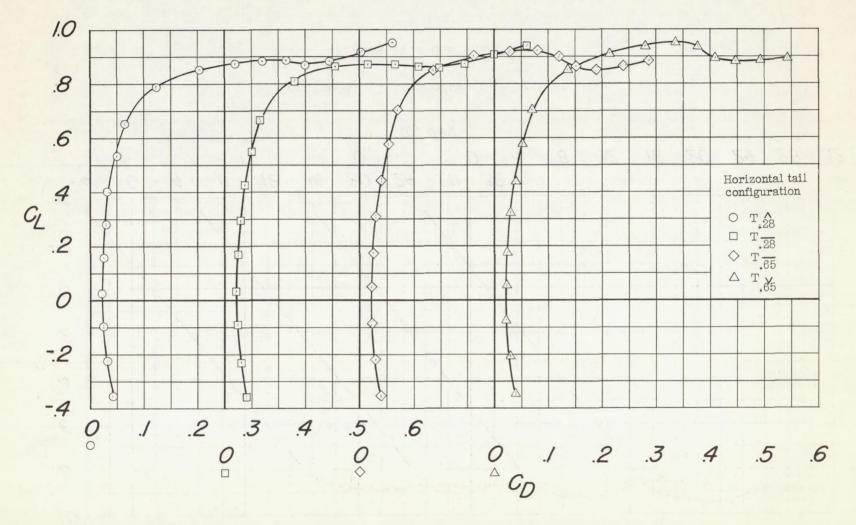


(a) Continued. Inlets off, C_m against C_L . Figure 17.- Continued.



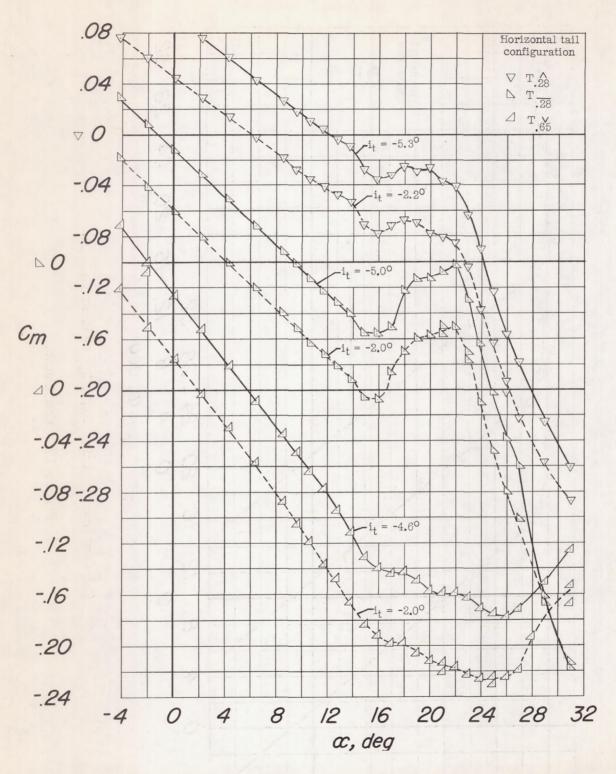
(a) Continued. Inlets off, \textbf{C}_{L} against $\alpha.$

Figure 17 .- Continued.

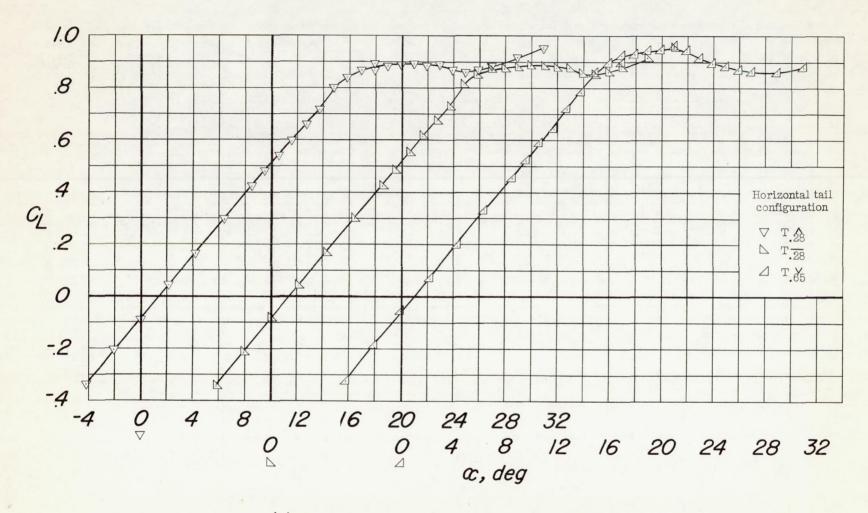


(a) Concluded. Inlets off, $C_{\rm L}$ against $C_{\rm D}$.

Figure 17.- Continued.

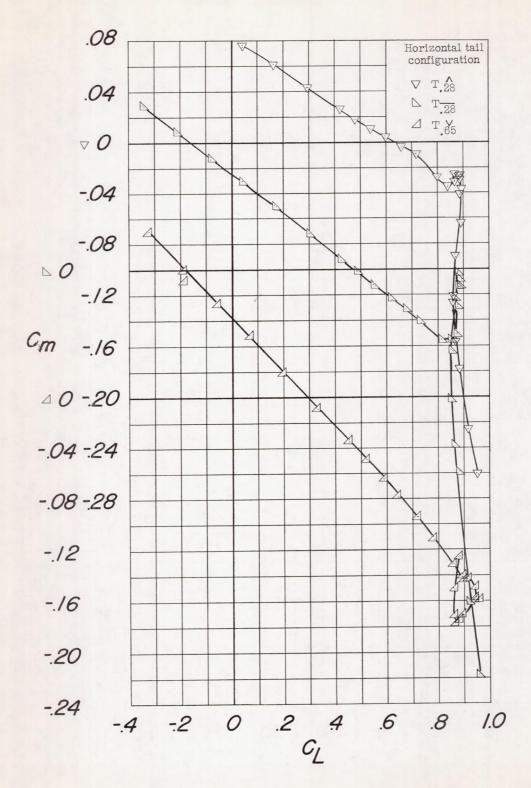


(b) Inlet D_3 , C_m against α .

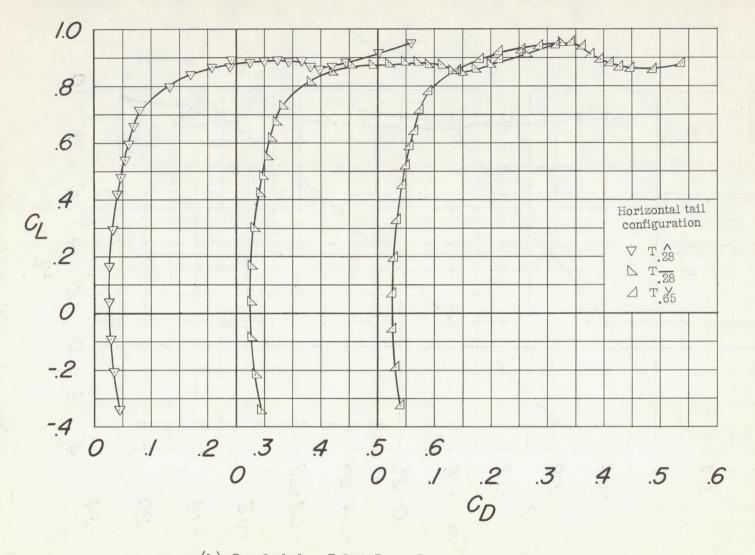


(b) Continued. Inlet D3, C_{L} against $\alpha.$

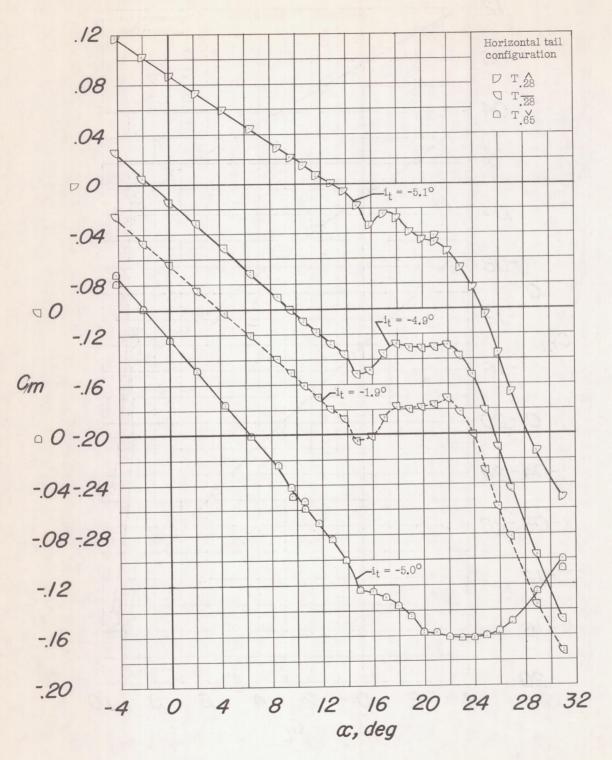
Figure 17.- Continued.



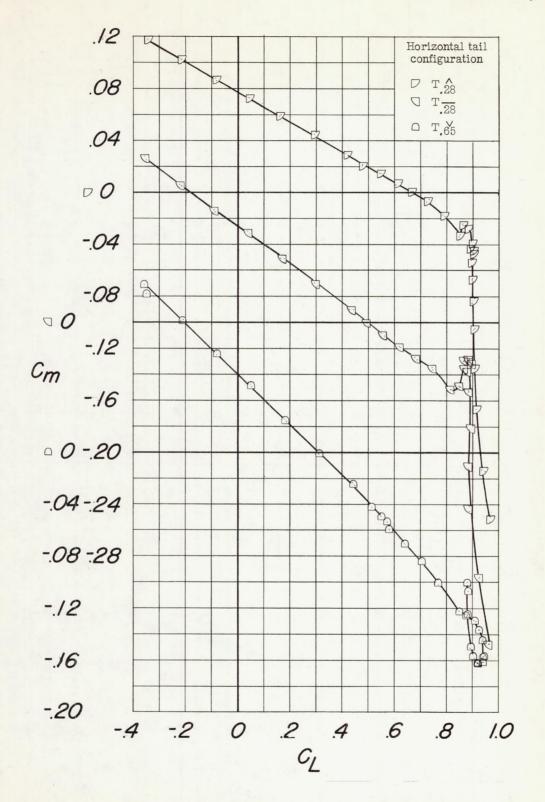
(b) Continued. Inlet D3, $C_{\rm m}$ against $C_{\rm L}$. Figure 17.- Continued.



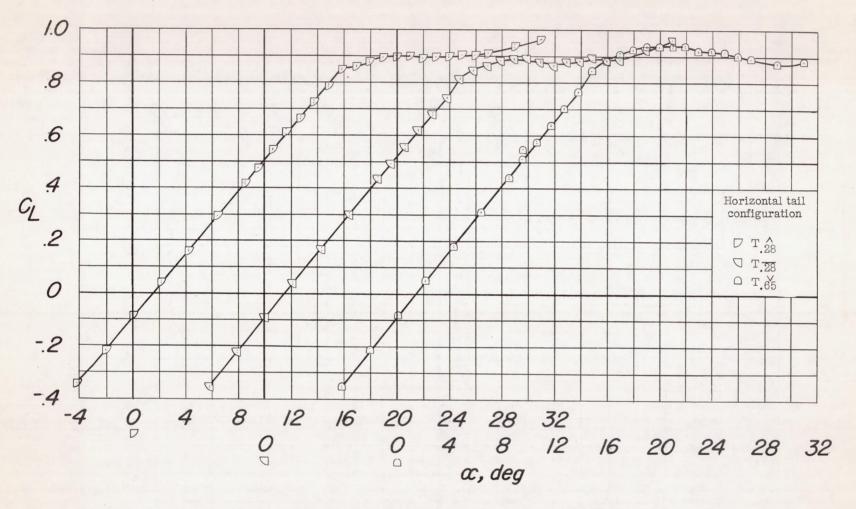
(b) Concluded. Inlet D3, $C_{\rm L}$ against $C_{\rm D}$.



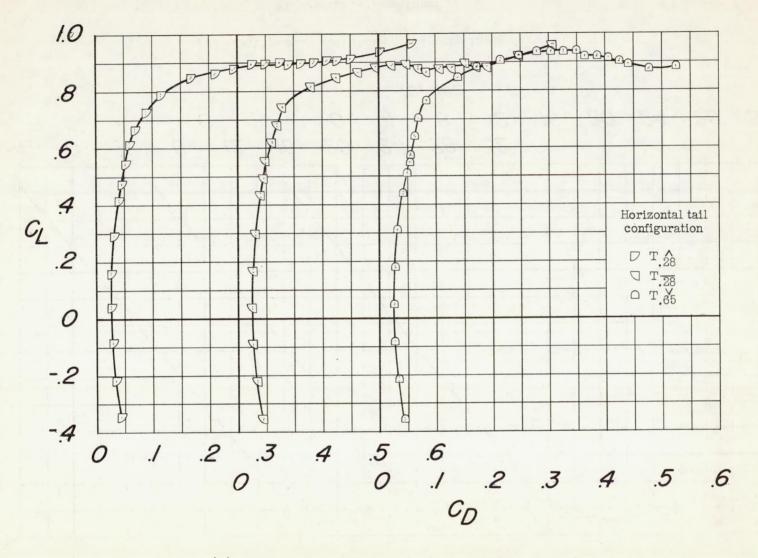
(c) Inlet D2, C_m against α . Figure 17.- Continued.



(c) Continued. Inlet ${\tt D_2},\ {\tt C_m}$ against ${\tt C_L}.$ Figure 17.- Continued.

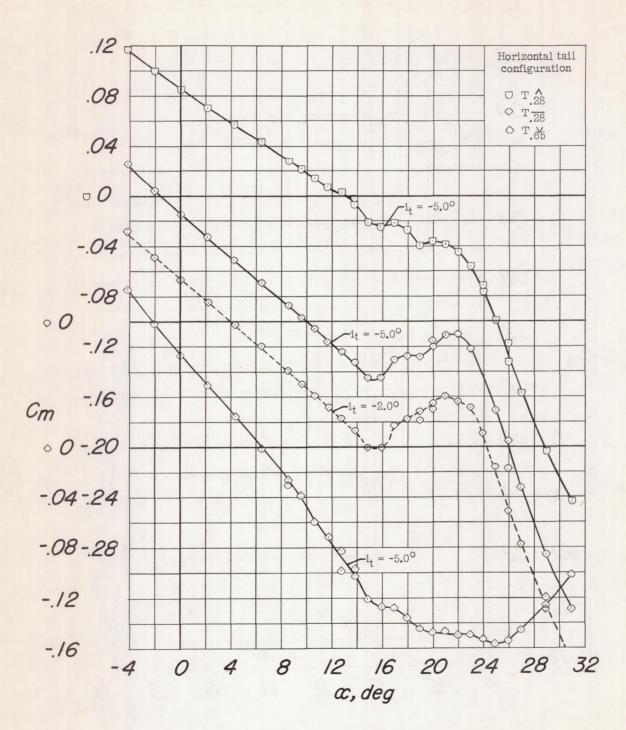


(c) Continued. Inlet $\textbf{D}_2,~\textbf{C}_L$ against $\alpha.$

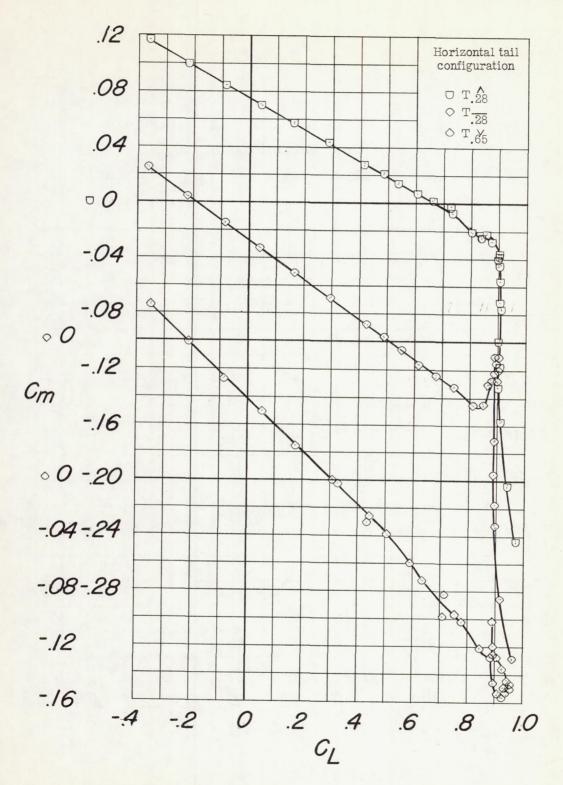


(c) Concluded. Inlet $\mathbf{D}_2, \ \mathbf{C}_L$ against $\mathbf{C}_D.$

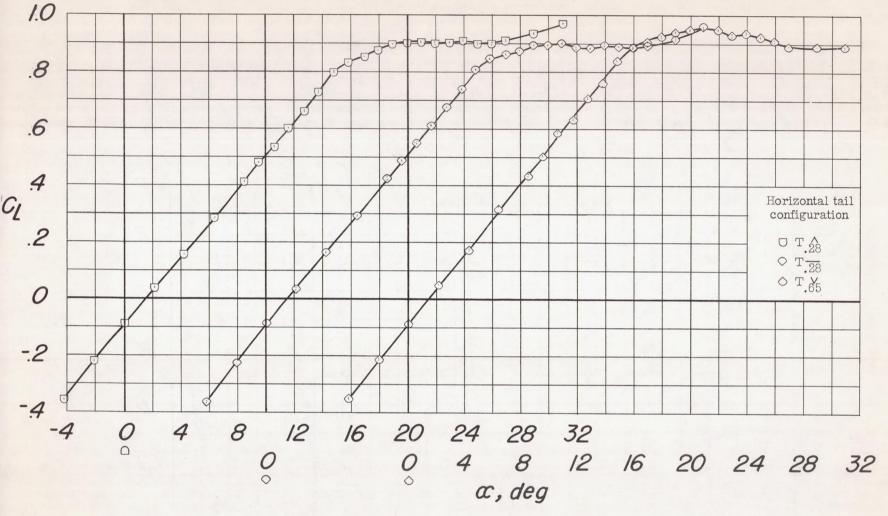
Figure 17 .- Continued.



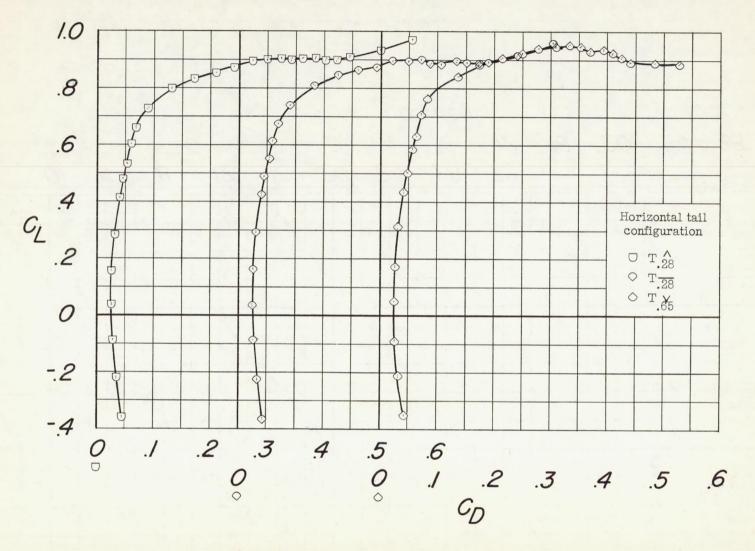
(d) Inlet D_1 , C_m against α . Figure 17.- Continued.



(d) Continued. Inlet D1, C_m against C_L .

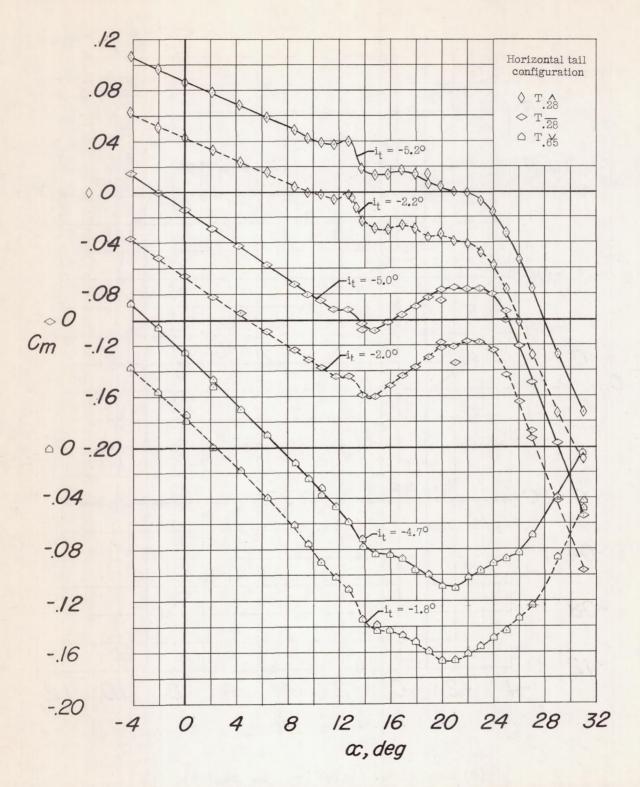


(d) Continued. Inlet $\textbf{D}_{1},~\textbf{C}_{L}$ against $\alpha.$

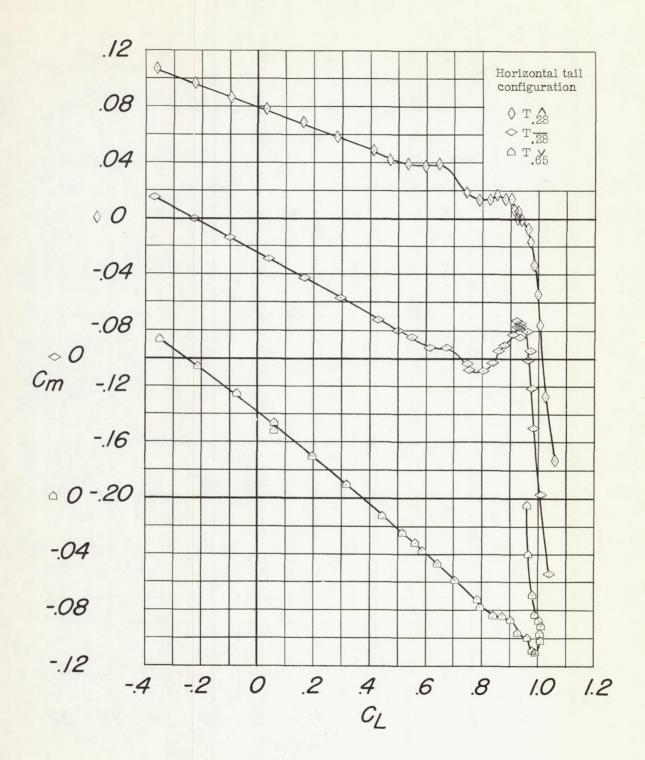


(d) Concluded. Inlet D_1 , C_L against C_D .

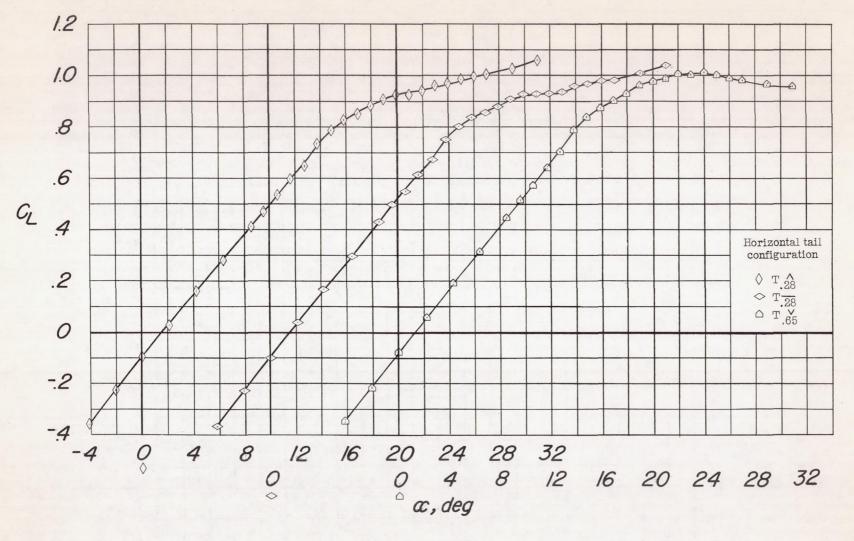
Figure 17 .- Continued.



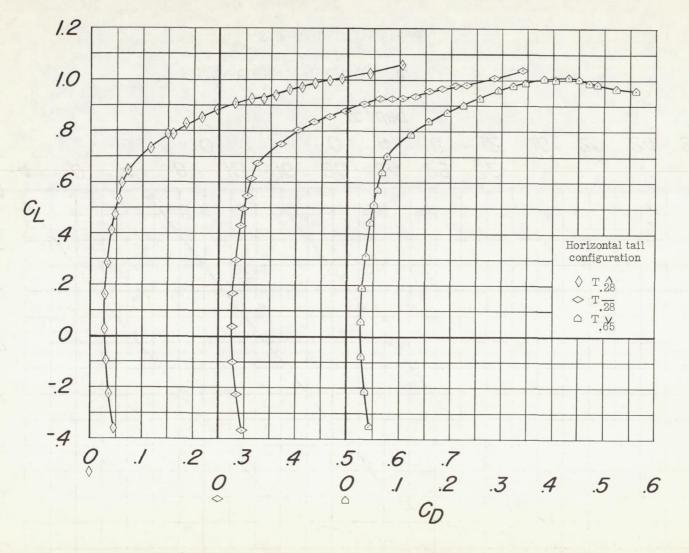
(e) Inlet D_0 , C_m against α .



(e) Continued. Inlet D_{O} , C_{m} against C_{L} . Figure 17.- Continued.



(e) Continued. Inlet $\textbf{D}_{0},~\textbf{C}_{L}$ against $\alpha.$



(e) Concluded. Inlet $\mathbf{D}_{O}, \quad \mathbf{C}_{L}$ against $\mathbf{C}_{D}.$

Figure 17.- Concluded.

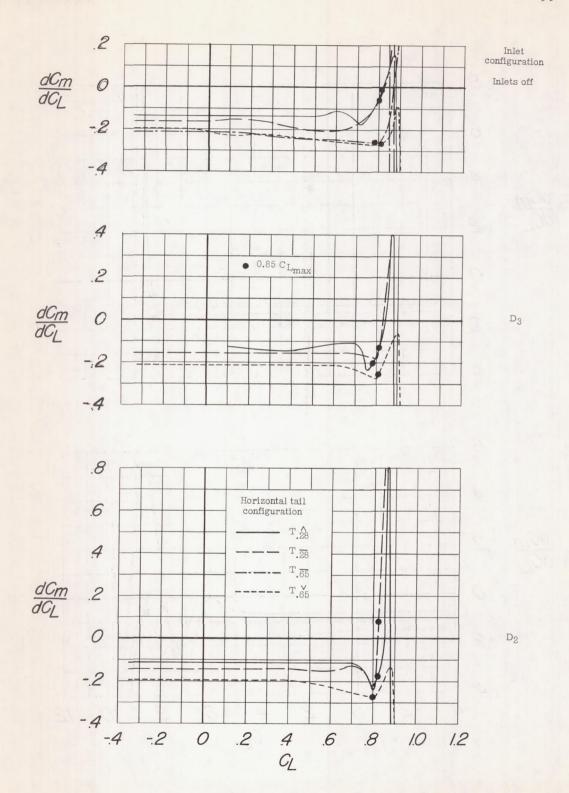


Figure 18.- The variation of dC_m/dC_L with lift coefficient for the model equipped with various horizontal-tail arrangements and with and without various inlets.

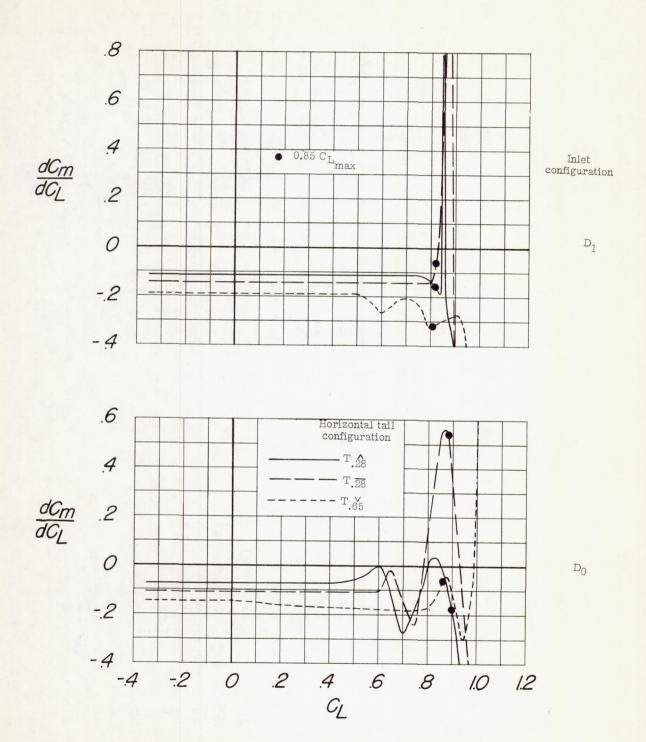
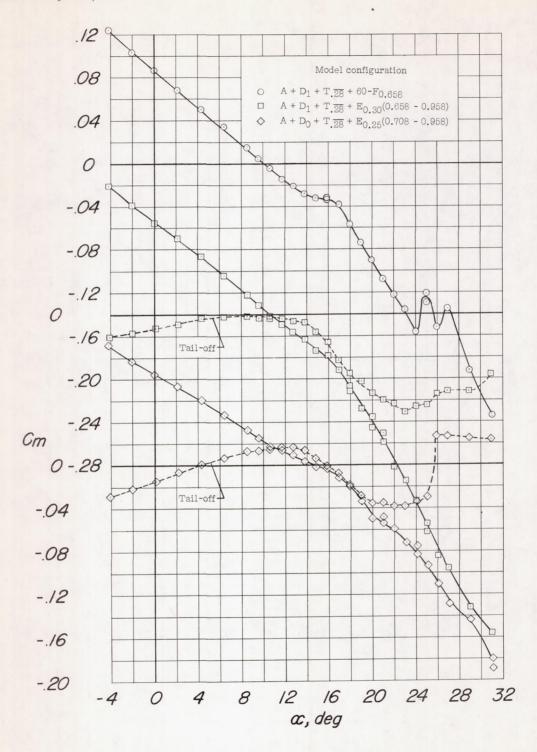
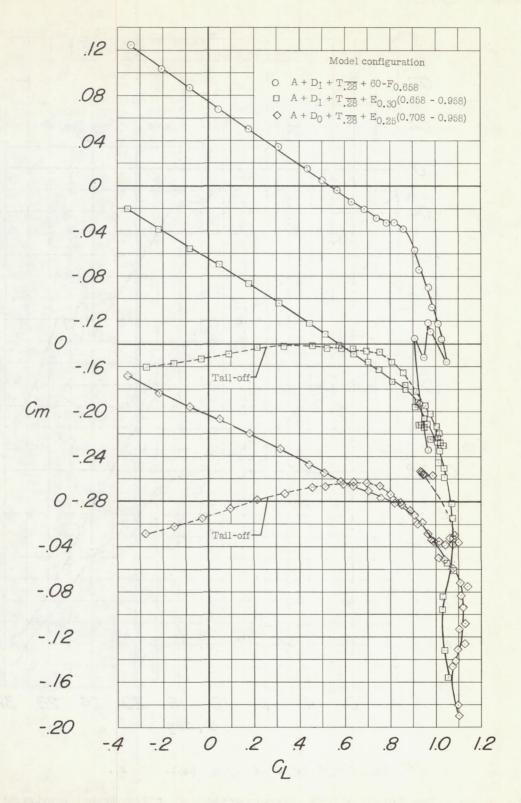


Figure 18.- Concluded.



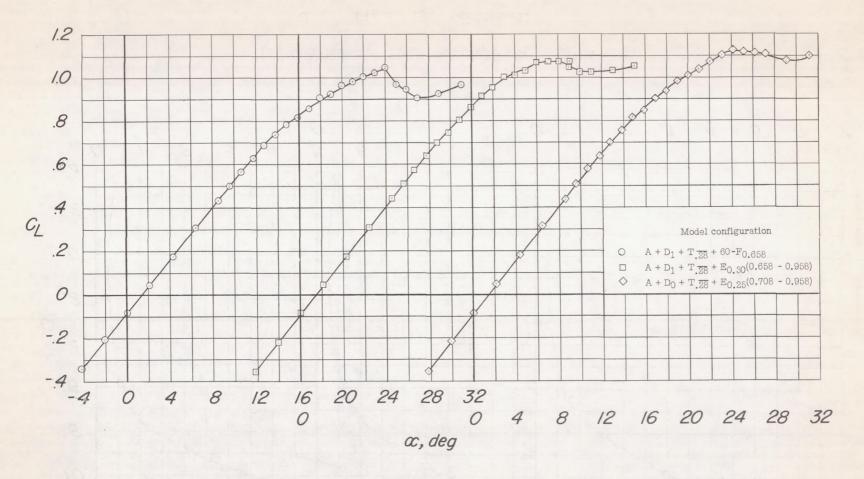
(a) Flaps neutral, C_m against α .

Figure 19.- The longitudinal characteristics of the model equipped with inlet D_1 or D_0 , horizontal tail $T_{\overline{28}}$, and various favorable wing configurations.

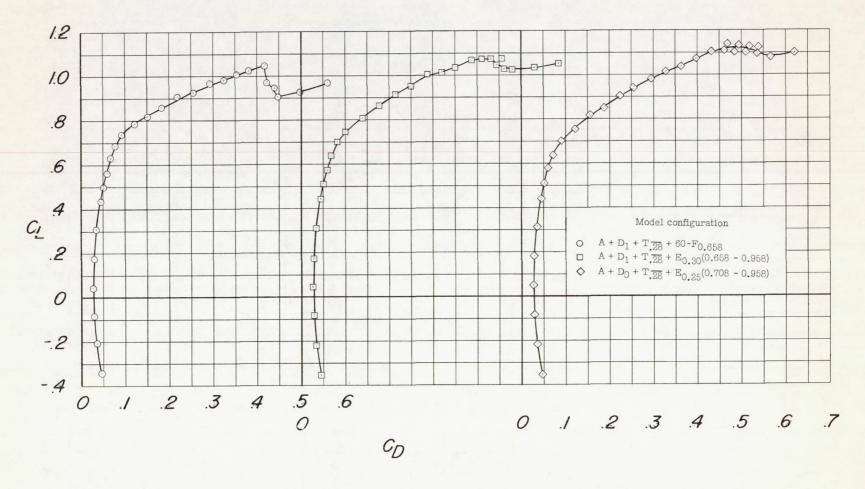


(a) Continued. Flaps neutral, C_m against C_L.

Figure 19.- Continued.

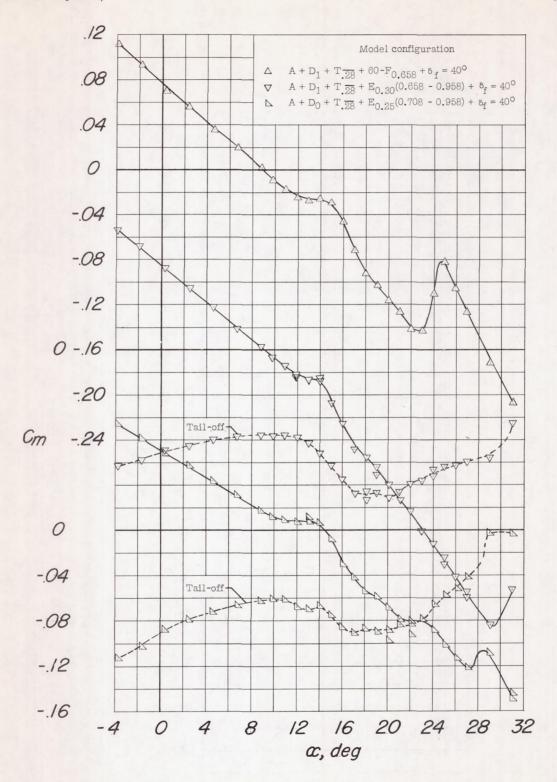


(a) Continued. Flaps neutral, C_{L} against $\alpha.$



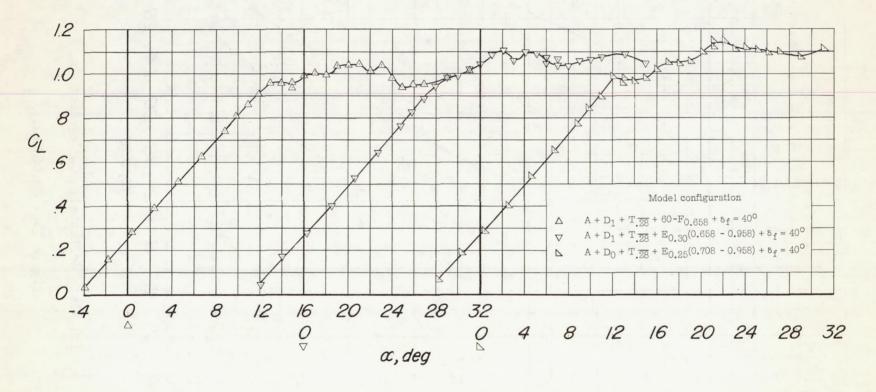
(a) Concluded. Flaps neutral, $C_{\rm L}$ against $C_{\rm D}$.

Figure 19.- Continued.



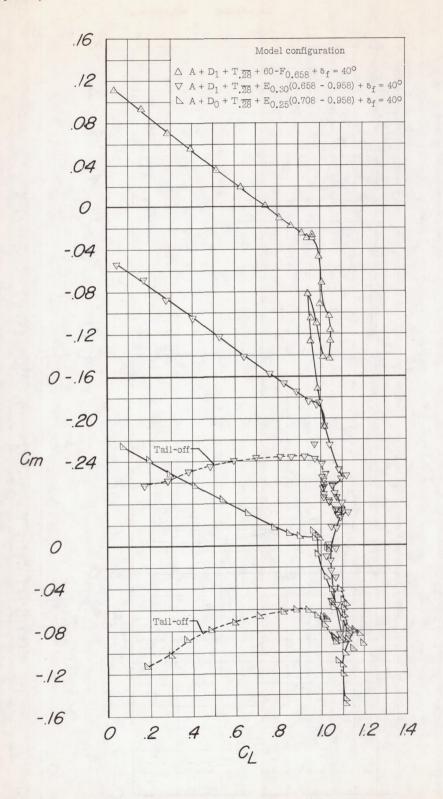
(b) Flaps deflected, $C_{\rm m}$ against α .

Figure 19.- Continued.

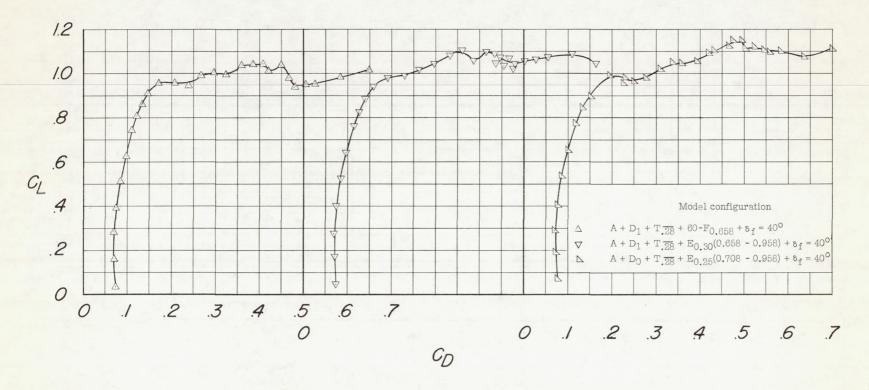


(b) Continued. Flaps deflected, $C_{\rm L}$ against α .

Figure 19.- Continued.

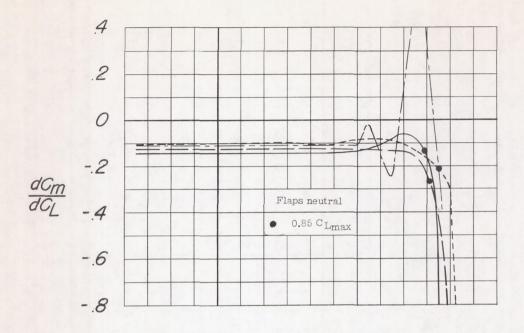


(b) Continued. Flaps deflected, $C_{\rm m}$ against $C_{\rm L}$. Figure 19.- Continued.



(b) Concluded. Flaps deflected, C_{L} against $\text{C}_{\text{D}}.$

Figure 19.- Concluded.



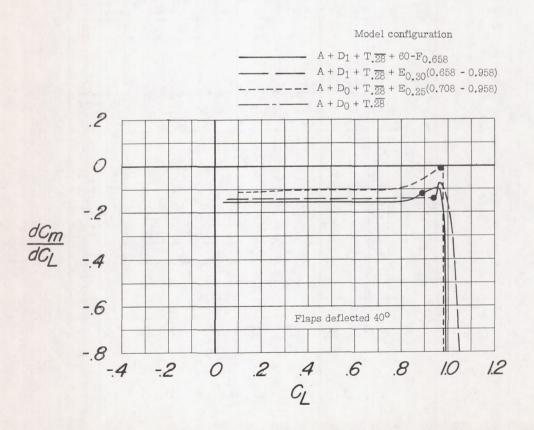


Figure 20.- Variation of dC_m/dC_L with lift coefficient for the model equipped with inlet D_1 or D_0 , horizontal tail $T_{.\overline{28}}$, and various favorable wing configurations.

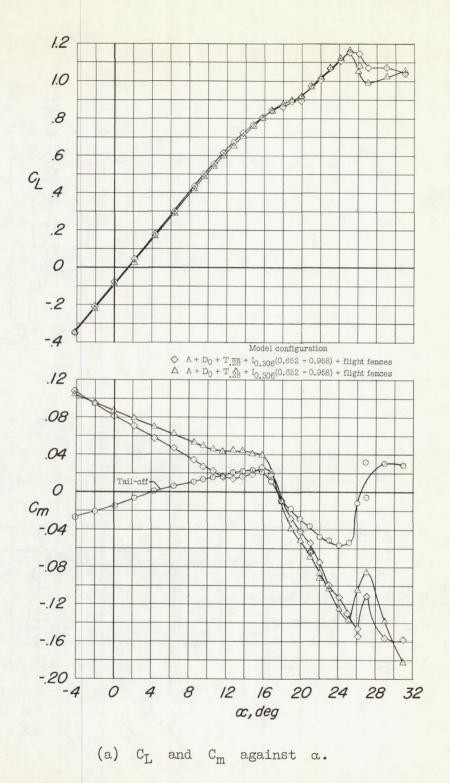
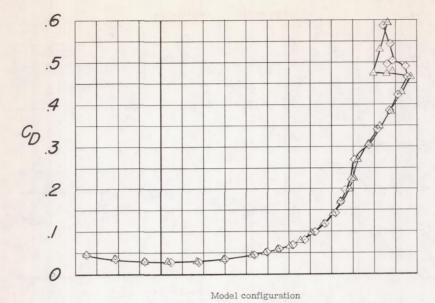
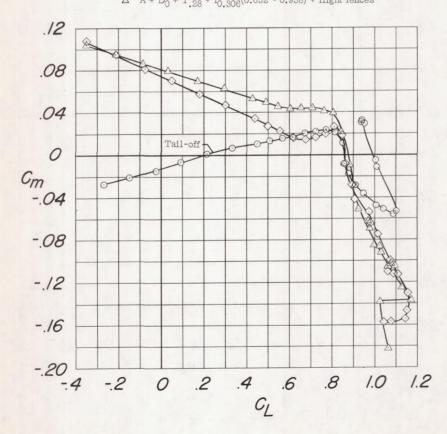


Figure 21.- The longitudinal characteristics of the model equipped with inlet D_0 , flight fences, leading-edge modification, and production or drooped tail. Trailing-edge flaps neutral.

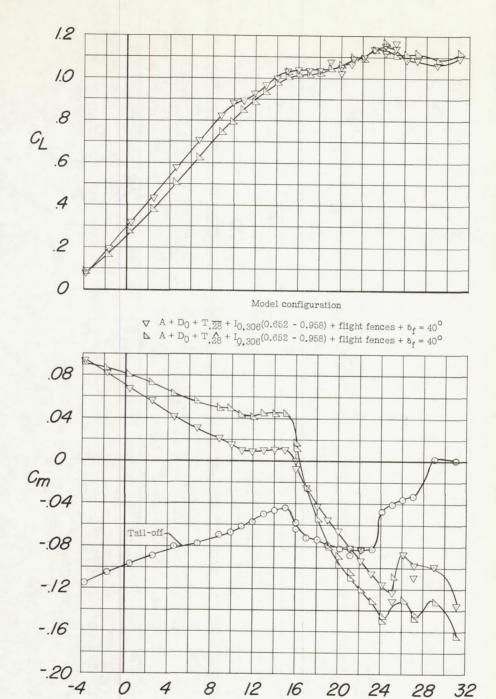


 \triangle A + D₀ + T. $\frac{1}{28}$ + I_{0.306}(0.652 - 0.958) + flight fences \triangle A + D₀ + T. $\frac{1}{28}$ + I_{0.306}(0.652 - 0.958) + flight fences



(b) C_{D} and C_{m} against $C_{\mathrm{L}}.$

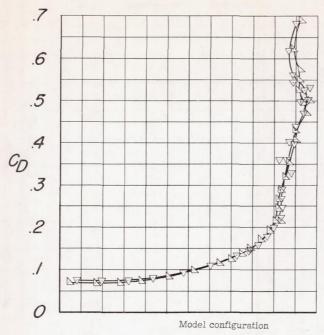
Figure 21 .- Concluded.



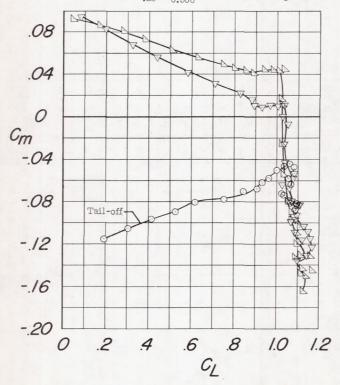
(a) \textbf{C}_{L} and \textbf{C}_{m} against $\alpha.$

æ, deg

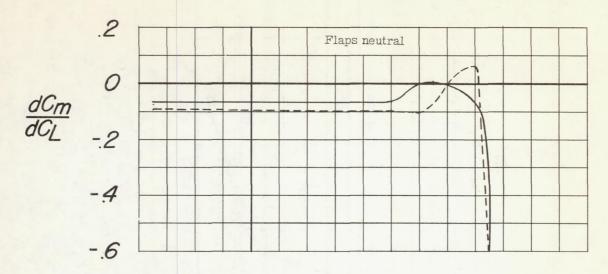
Figure 22.- The longitudinal characteristics of the model equipped with inlet D_0 , flight fences, leading-edge modification, and production or drooped tail. Trailing-edge flaps deflected 40° .



 $\begin{array}{ll} \boldsymbol{\nabla} & A + D_0 + T.\overline{28} + I_{0.306} (0.652 - 0.958) + \text{flight fences} + \delta_f = 40^{\circ} \\ \boldsymbol{\triangle} & A + D_0 + T.\underline{28} + I_{0.306} (0.652 - 0.958) + \text{flight fences} + \delta_f = 40^{\circ} \end{array}$



(b) C_{D} and C_{m} against C_{L} . Figure 22.- Concluded.



Model configuration

A + D₀ + T_{.28} + I_{0.306}(0.652 - 0.958) + flight fences A + D₀ + T_{.28} + I_{0.306}(0.652 - 0.958) + flight fences

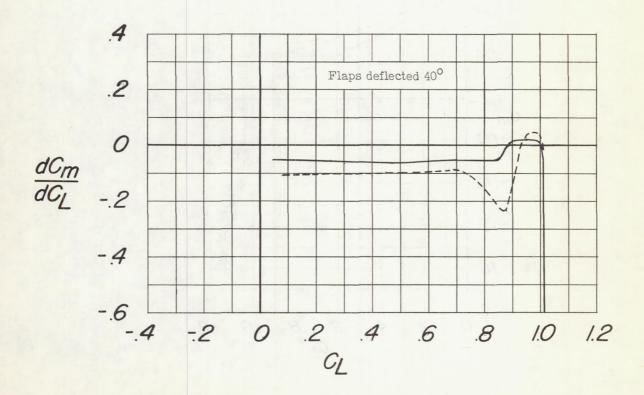
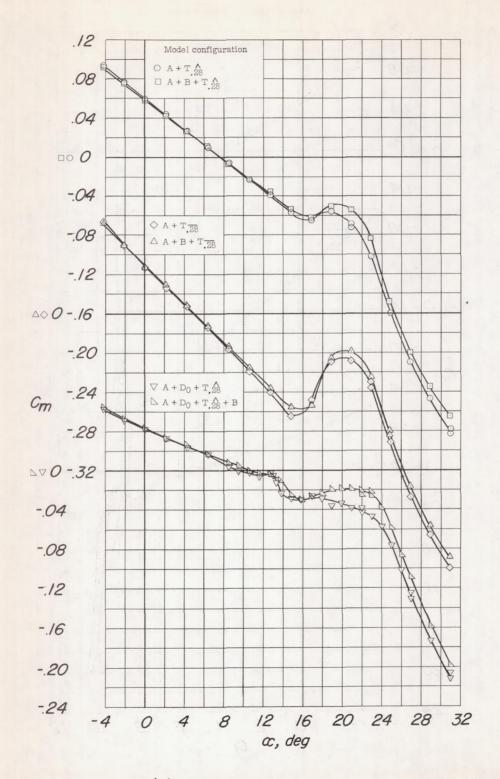
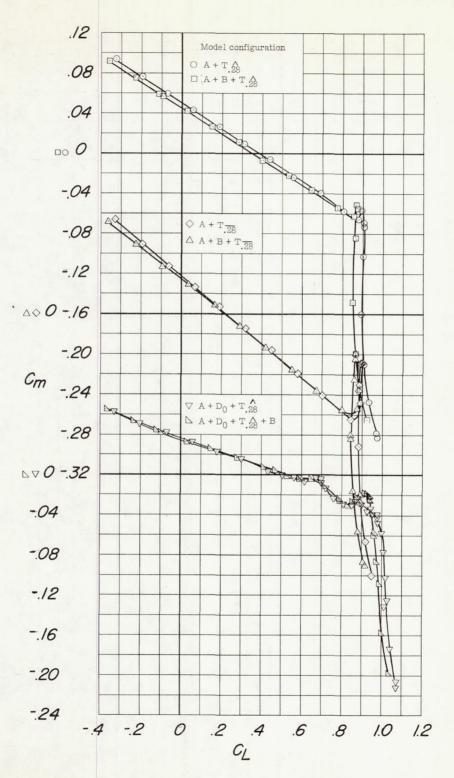


Figure 23.- The variation of dC_m/dC_L with lift coefficient for the model equipped with inlet D_0 , flight fences, leading-edge modification, and the production or drooped tail.



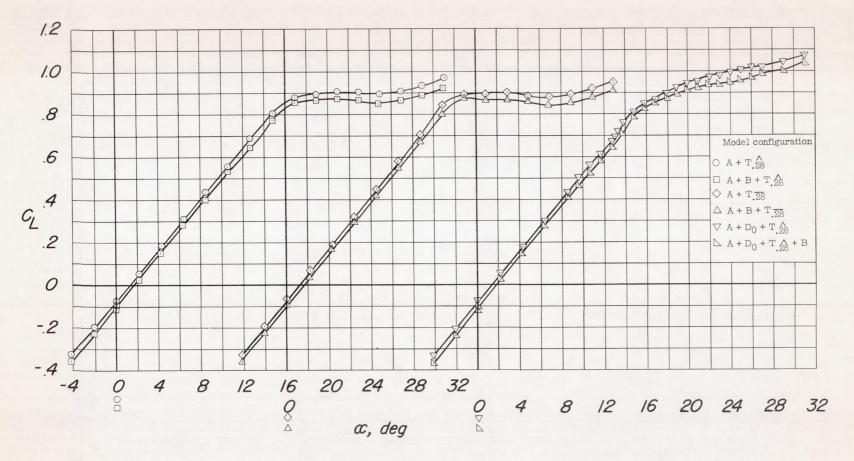
(a) C_m against α .

Figure 24.- Effect of external stores on the longitudinal characteristics of the model equipped with various tails in inlet configurations.



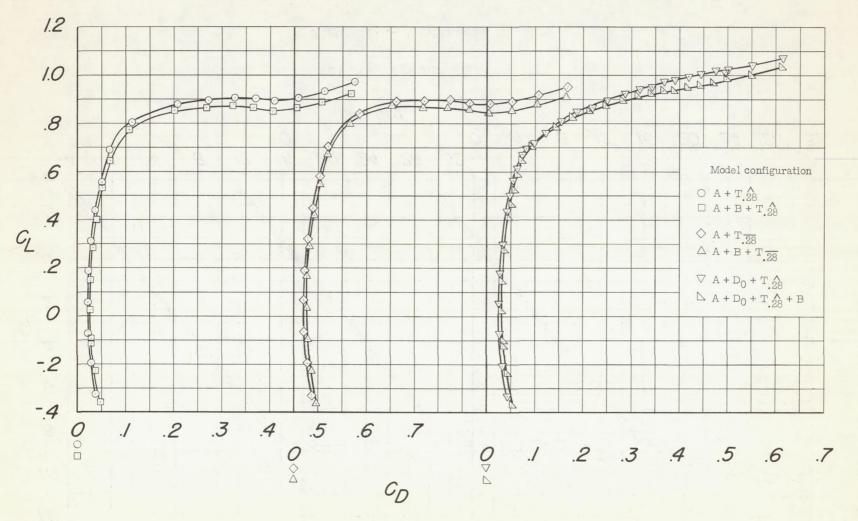
(b) $C_{\rm m}$ against $C_{\rm L}$.

Figure 24.- Continued.



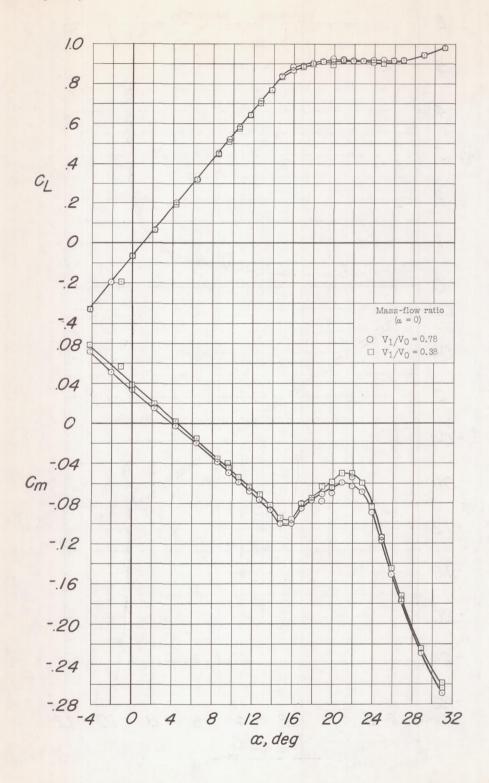
(c) C_L against α .

Figure 24.- Continued.



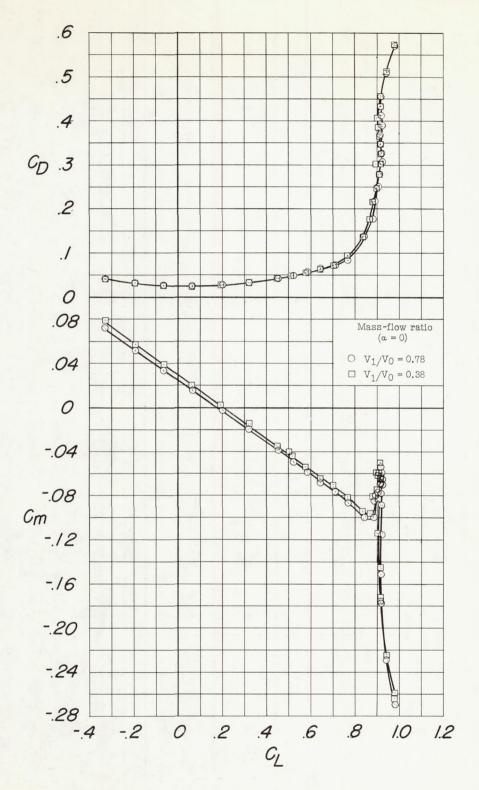
(d) C_{L} against C_{D} .

Figure 24.- Concluded.

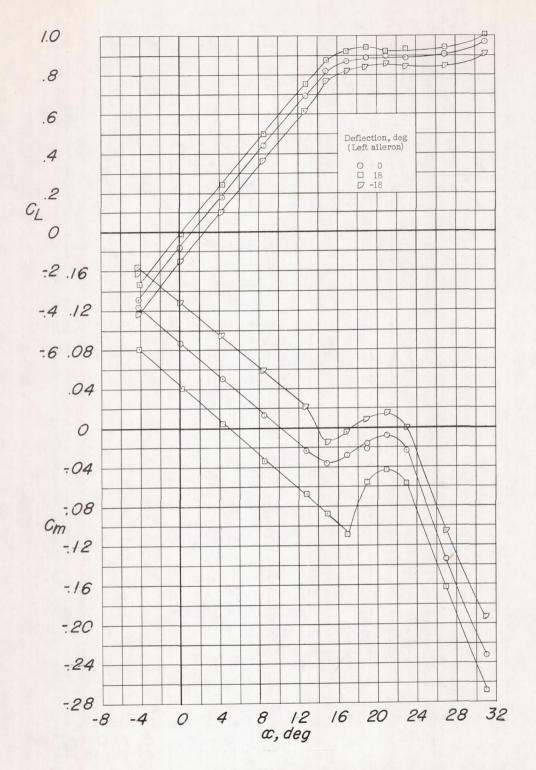


(a) C_{L} and C_{m} against $\alpha.$

Figure 25.- Effect of inlet mass-flow ratio on the longitudinal characteristics of the model equipped with inlet D_1 and horizontal tail $T_{\overline{28}}$.

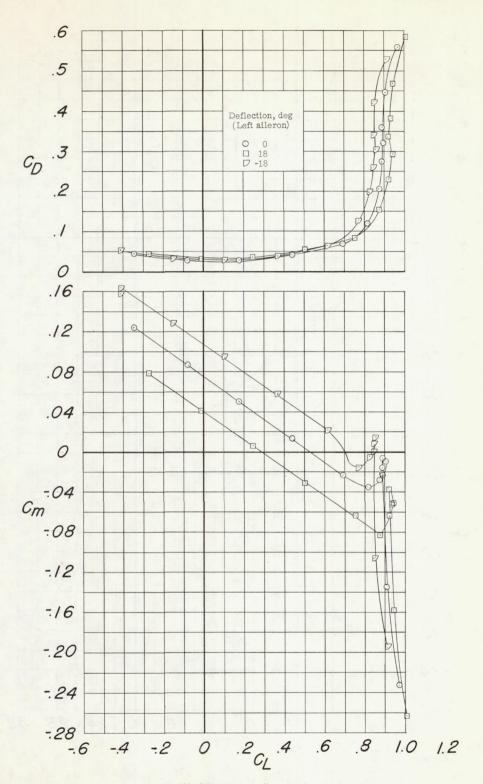


(b) $C_{\rm D}$ and $C_{\rm m}$ against $C_{\rm L}$. Figure 25.- Concluded.

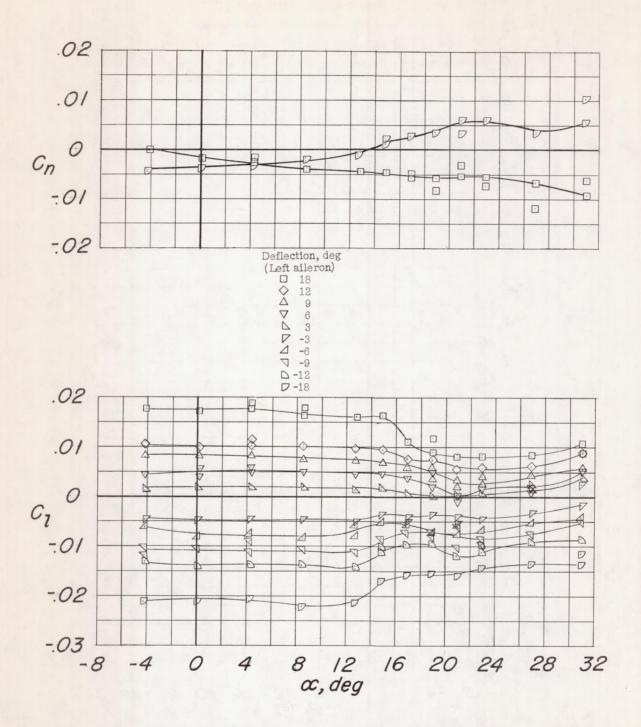


(a) C_{L} and C_{m} against $\alpha.$

Figure 26.- Longitudinal and lateral-control characteristics of the model equipped with an outboard aileron. Configuration A + D₁ + $\frac{T}{.28}$.

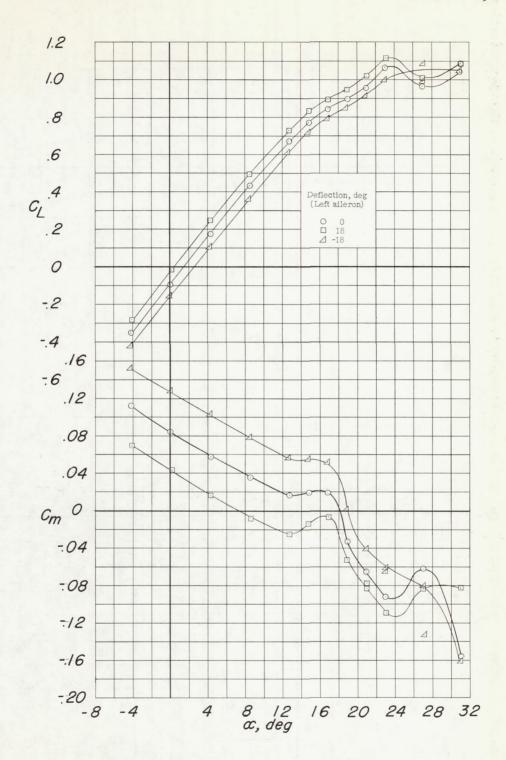


(b) C_{D} and C_{m} against $C_{\mathrm{L}}.$ Figure 26.- Continued.



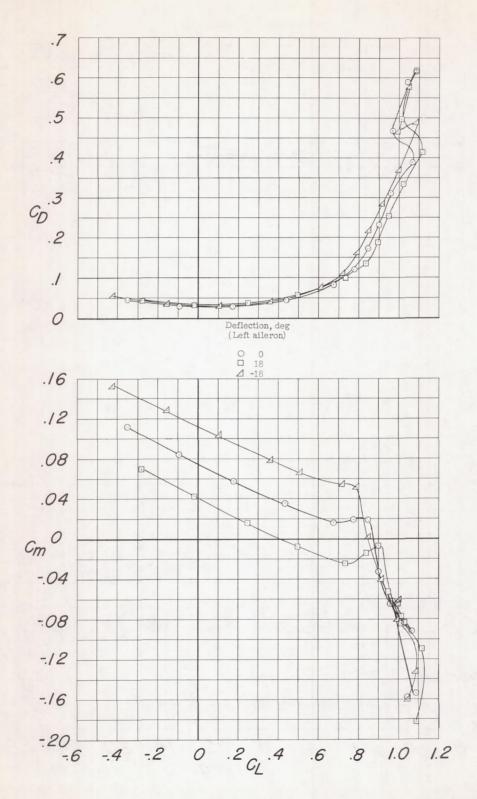
(c) C_n and C_l against α .

Figure 26.- Concluded.

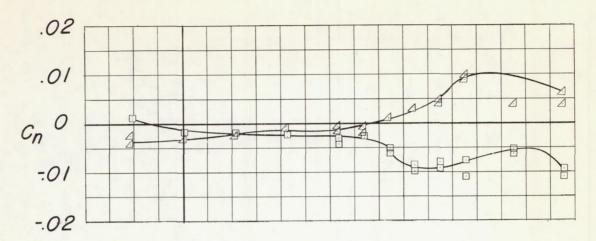


(a) \textbf{C}_{L} and \textbf{C}_{m} against $\alpha.$

Figure 27.- Longitudinal and lateral-control characteristics of the model equipped with an outboard aileron. Configuration A + D₀ + $T.\overline{28}$ + $I_{0.306}(0.652 - 0.958)$ + flight fences.

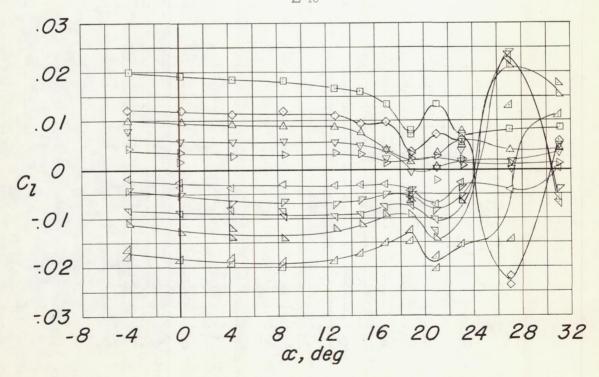


(b) ${\rm C_D}$ and ${\rm C_m}$ against ${\rm C_L}.$ Figure 27.- Continued.



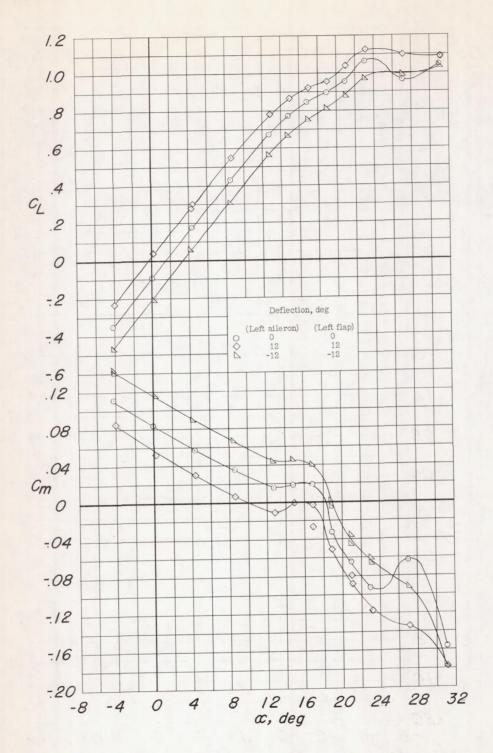
Deflection, deg (Left aileron)

□ 18
♦ 12
Δ 9
∇ 6
▷ 3
∇ -6
∇ -9
Δ -12
□ -18



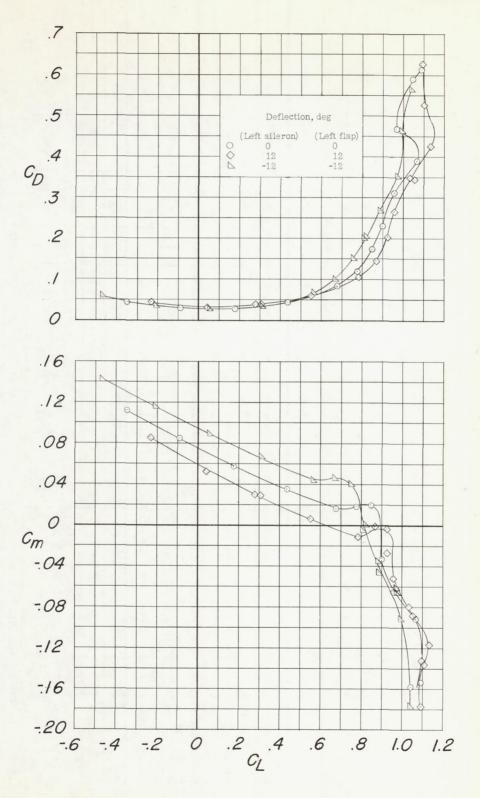
(c) C_n and C_l against α .

Figure 27.- Concluded.

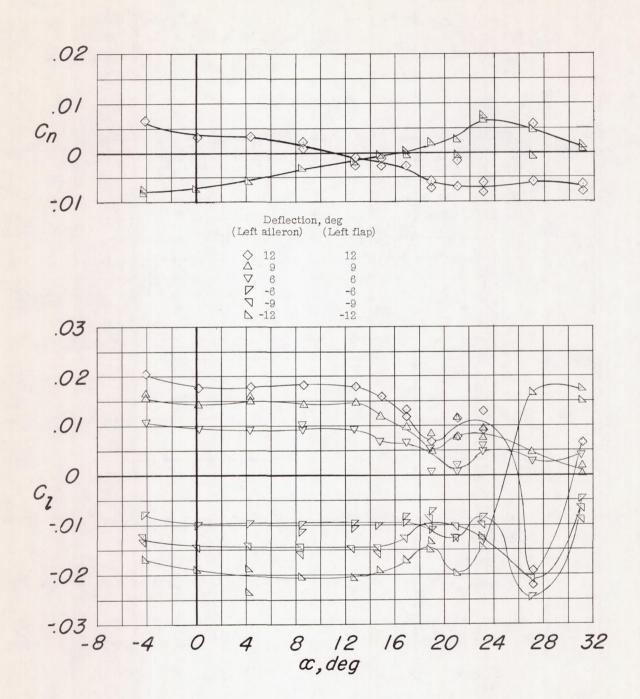


(a) $C_{\rm L}$ and $C_{\rm m}$ against α .

Figure 28.- Longitudinal and lateral-control characteristics of the model equipped with a full-span aileron. Configuration A + D $_0$ + T $_{\overline{28}}$ + I $_{0.306}$ (0.652 - 0.958) + flight fences.

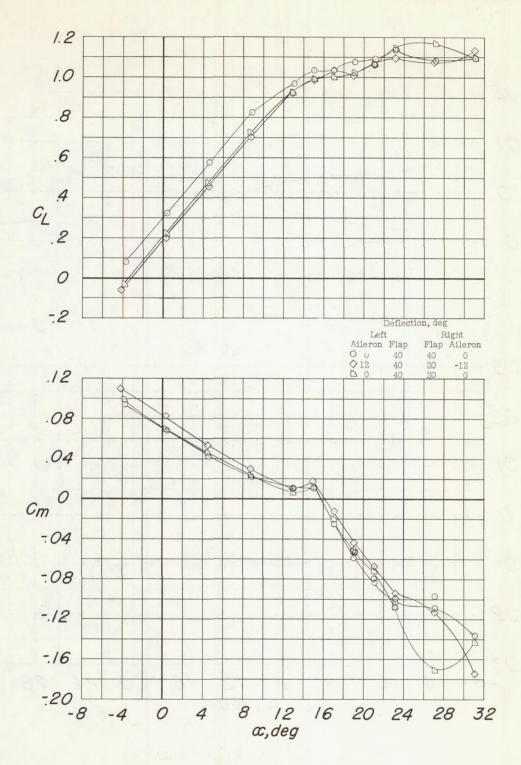


(b) C_{D} and C_{m} against C_{L} . Figure 28.- Continued.



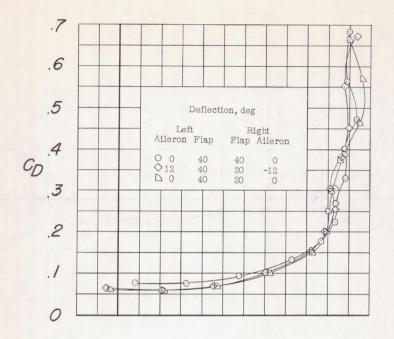
(c) C_n and C_l against α .

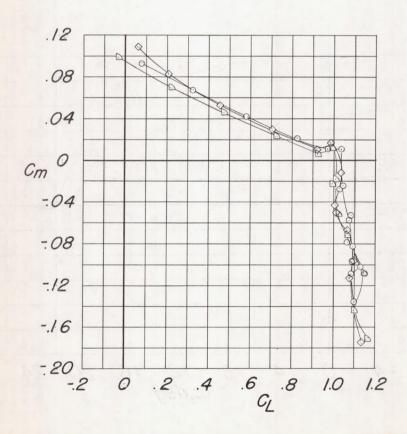
Figure 28.- Concluded.



(a) $C_{\rm L}$ and $C_{\rm m}$ against α .

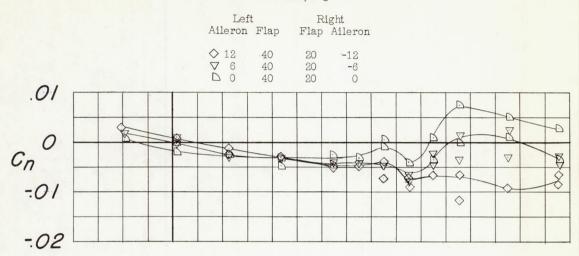
Figure 29.- Longitudinal and lateral-control characteristics of the model equipped with differentially deflected flaps and outboard ailerons. Configuration A + D $_0$ + T $_{.\overline{28}}$ + I $_{0.306}$ (0.652 - 0.958) + flight fences.

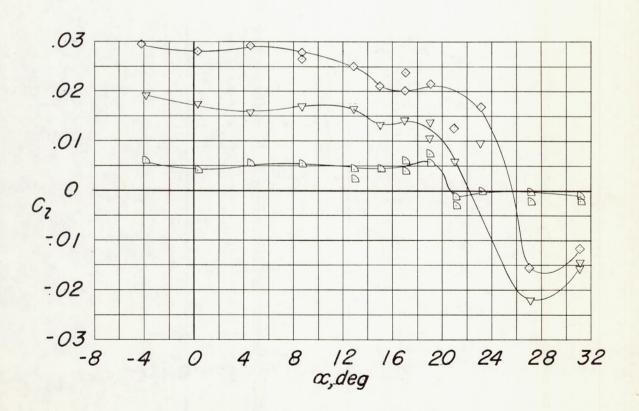




(b) $C_{\rm D}$ and $C_{\rm m}$ against $C_{\rm L}$. Figure 29.- Continued.

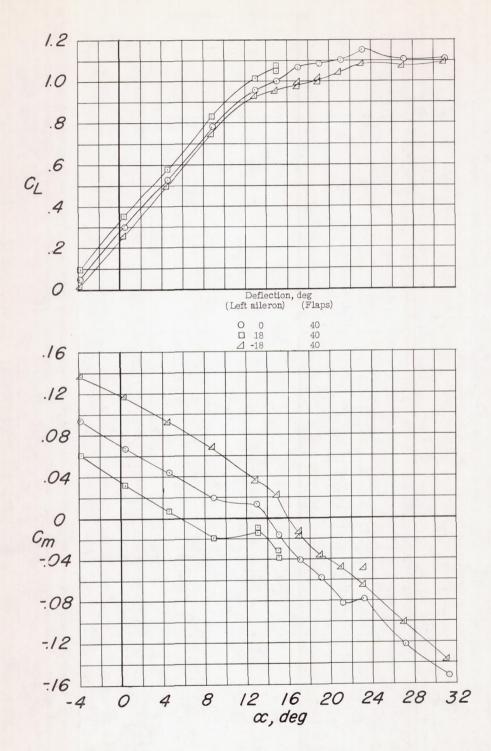
Deflection, deg





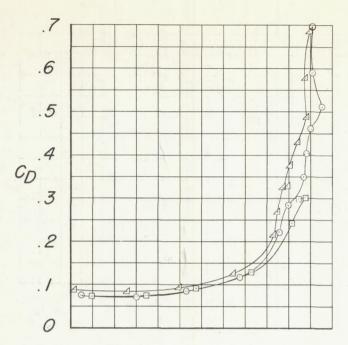
(c) C_n and C_l against α .

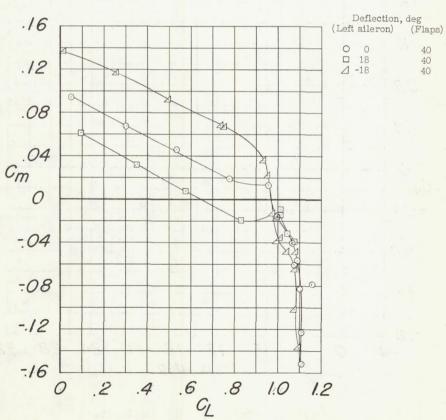
Figure 29 .- Concluded.



(a) $C_{\rm L}$ and $C_{\rm m}$ against α .

Figure 30.- Longitudinal and lateral-control characteristics of the model equipped with an outboard aileron. Configuration A + D₀ + $\overline{T.28}$ + $E_{0.25}(0.708 - 0.958)$.

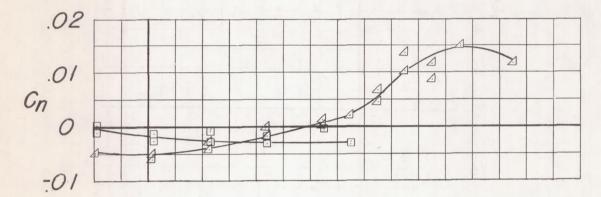


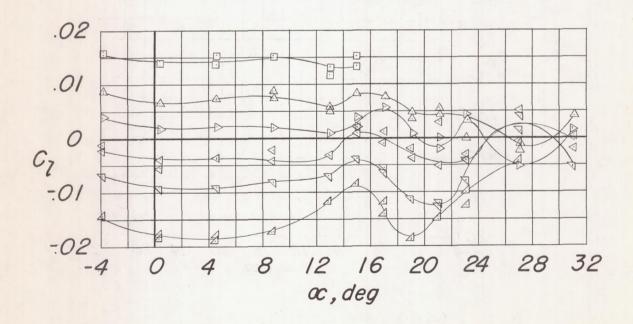


(b) $C_{
m D}$ and $C_{
m m}$ against $C_{
m L}$. Figure 30.- Continued.

	aileron)	
	18	40
\triangle	9	40
~	0	10

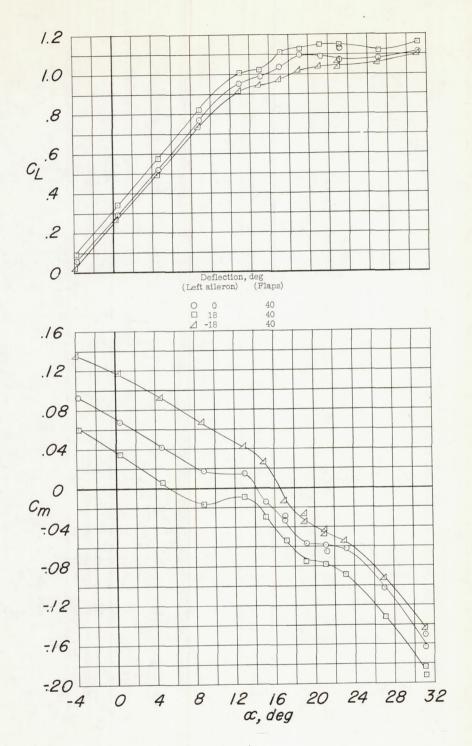
\triangle	9	40
D	3	40
\triangleleft	-3	40
1	-9	40
1	-18	40





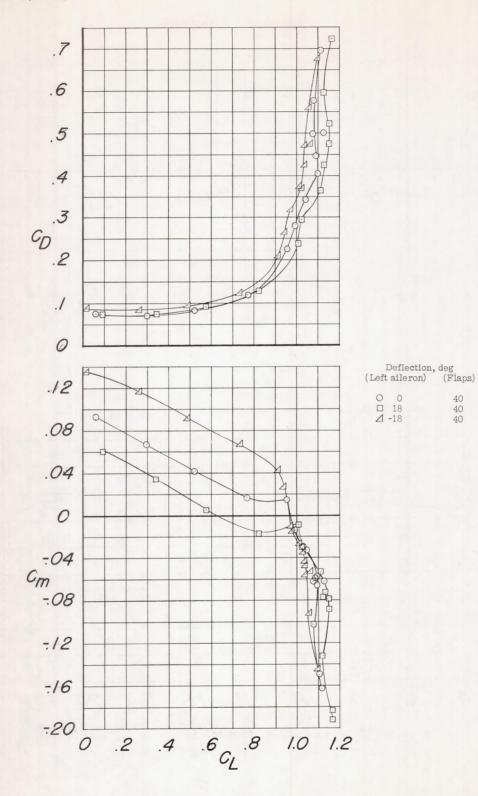
(c) C_n and C_l against α .

Figure 30.- Concluded.

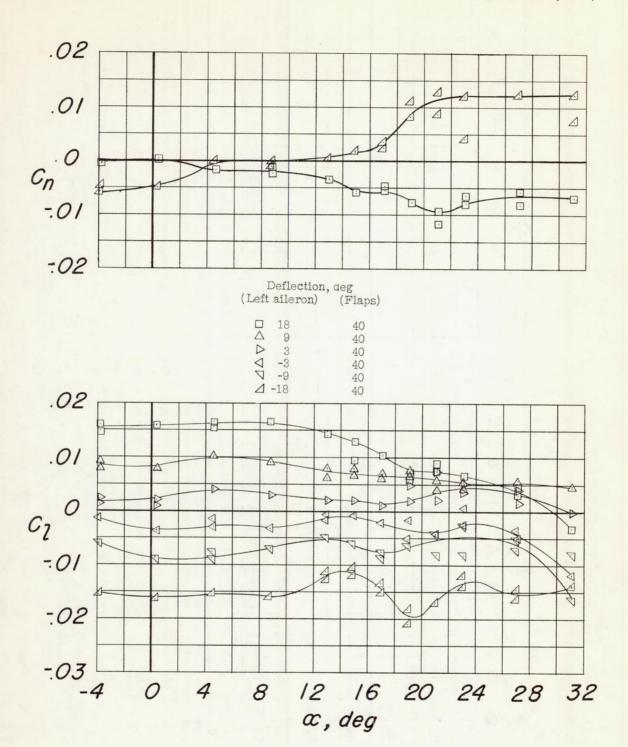


(a) $C_{\rm L}$ and $C_{\rm m}$ against α .

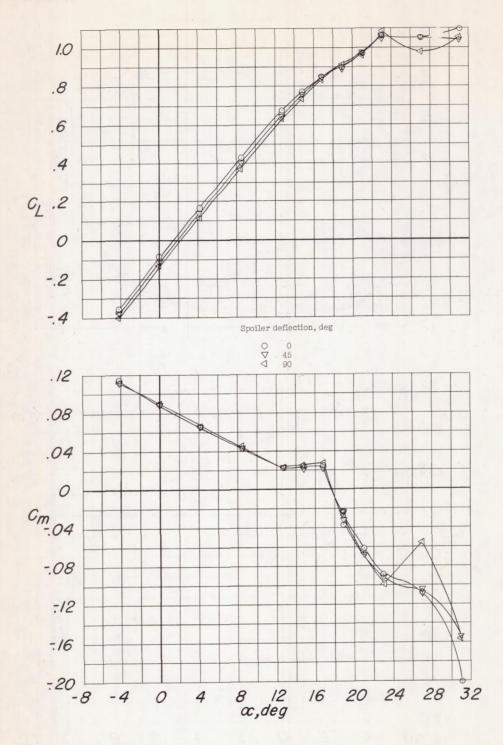
Figure 31.- Longitudinal and lateral-control characteristics of the model equipped with an outboard aileron. Configuration A + D₀ + $E_{0.15}(0.708b/2 \text{ to } 0.858b/2) + \delta_f = 40^{\circ}$.



(b) C_{D} and C_{m} against $C_{\mathrm{L}}.$ Figure 31.- Continued.

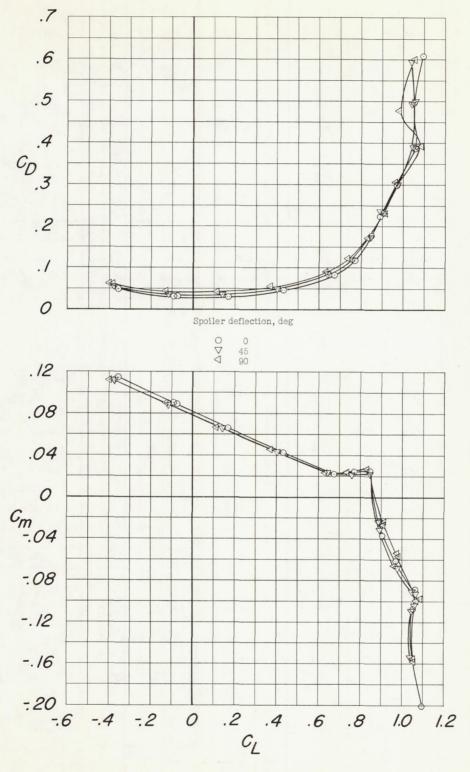


(c) C_n and C_l against α . Figure 31.- Concluded.

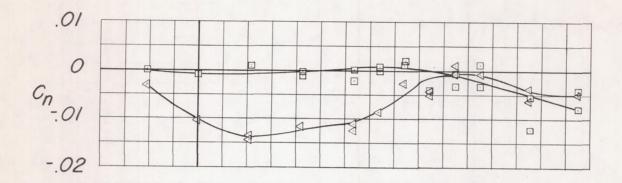


(a) \textbf{C}_{L} and \textbf{C}_{m} against $\alpha.$

Figure 32.- Longitudinal and lateral-control characteristics of the model equipped with solid flap-type spoilers. Configuration A + D_0 + $T.\overline{28}$ + I0.306(0.652 - 0.958) + flight fences.

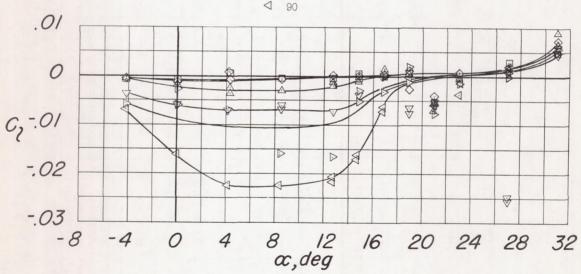


(b) C_{D} and C_{m} against C_{L} . Figure 32.- Continued.



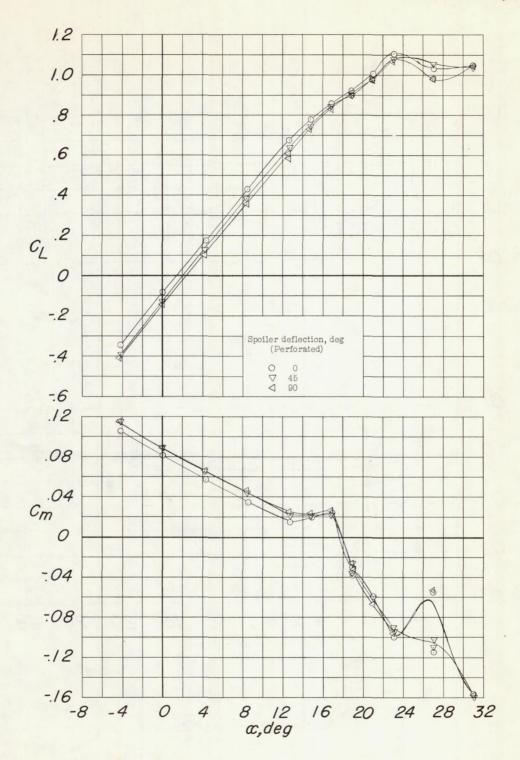
Spoiler deflection, deg





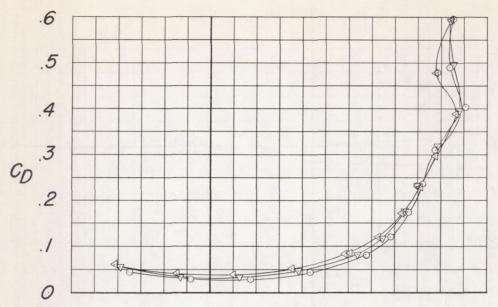
(c) C_n and C_l against α .

Figure 32.- Concluded.

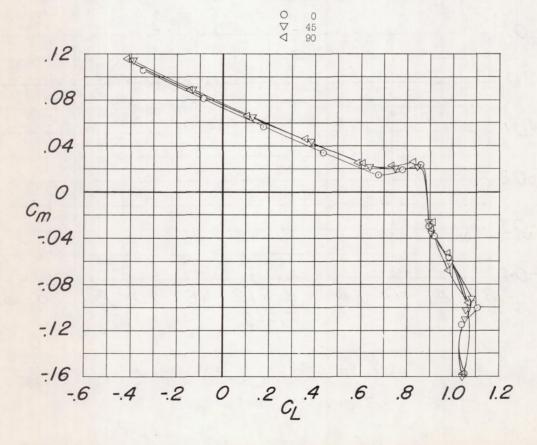


(a) C_L and C_m against α .

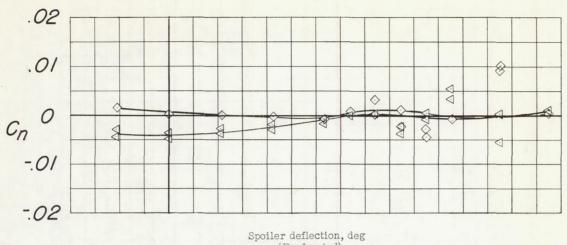
Figure 33.- Longitudinal and lateral-control characteristics of the model equipped with perforated flap-type spoilers. Configuration A + D₀ + $T.\overline{28} + I_{0.306}(0.652 - 0.958) + flight fences$.



Spoiler deflection, deg (Perforated)

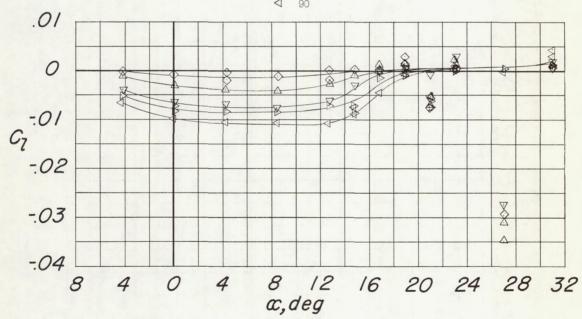


(b) C_{D} and C_{m} against C_{L} . Figure 33.- Continued.



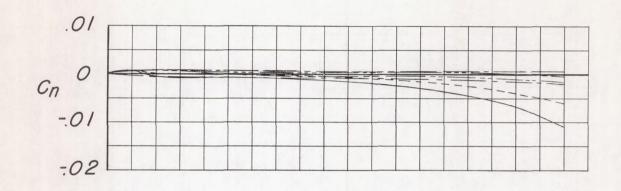
Spoiler deflection, deg (Perforated)

♦ 9.35
 △ 19
 ∇ 45
 ▷ 55
 ✓ 90



(c) C_n and C_l against α .

Figure 33.- Concluded.



(deg) Solid Perforated

12 ----16 ---20 ---

Spoilers

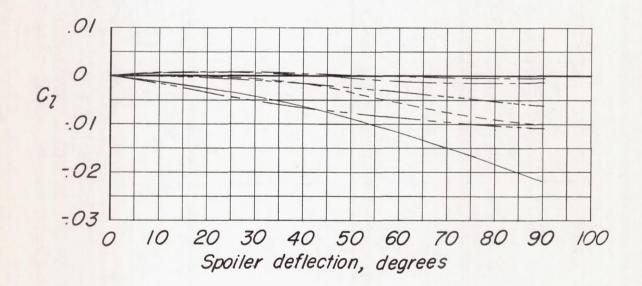
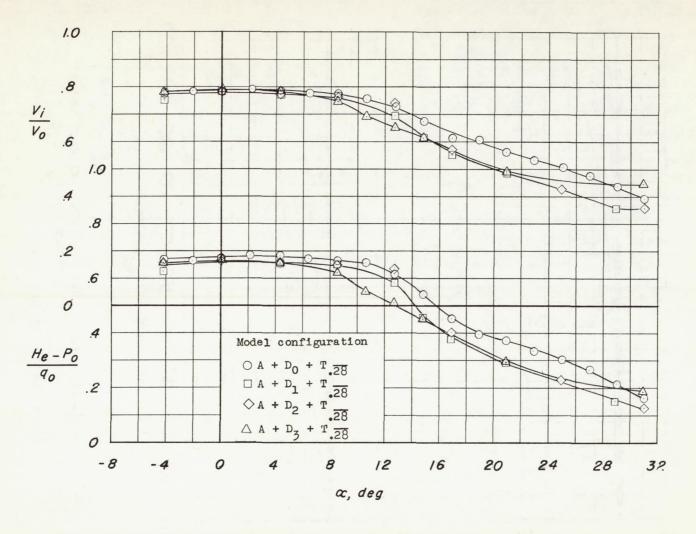
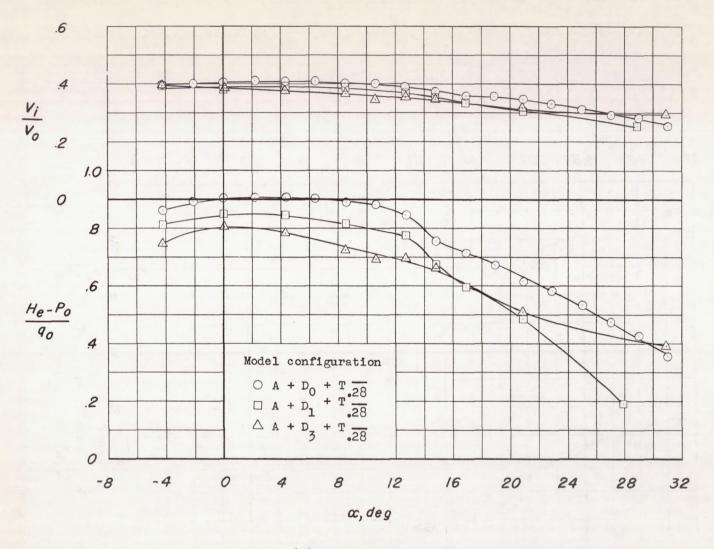


Figure 34.- Variations of the yaw and roll characteristics of the model with spoiler deflection. Configuration A + D $_0$ + T $_{.28}$ + I $_{0.306}$ (0.652 - 0.958) + flight fences.



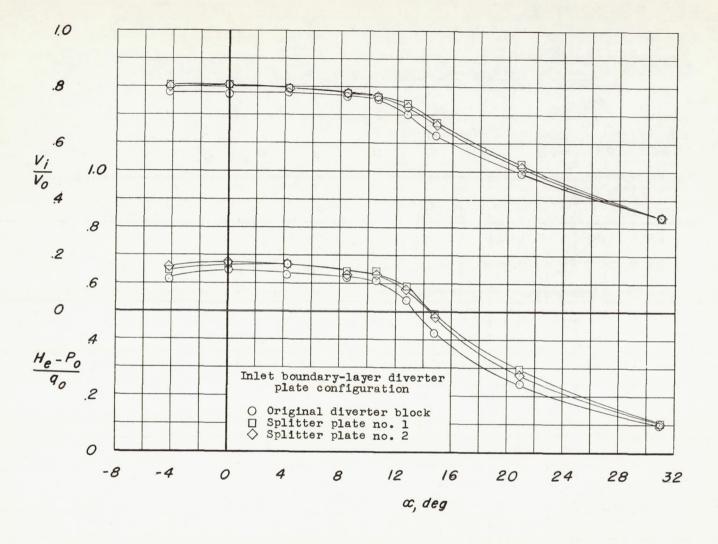
(a) Exit, full open.

Figure 35.- Variations of $\frac{V_1}{V_0}$ and $\frac{H_e - P_o}{q_o}$ with angle of attack for the model equipped with various inlets. $R = 9 \times 10^6$.



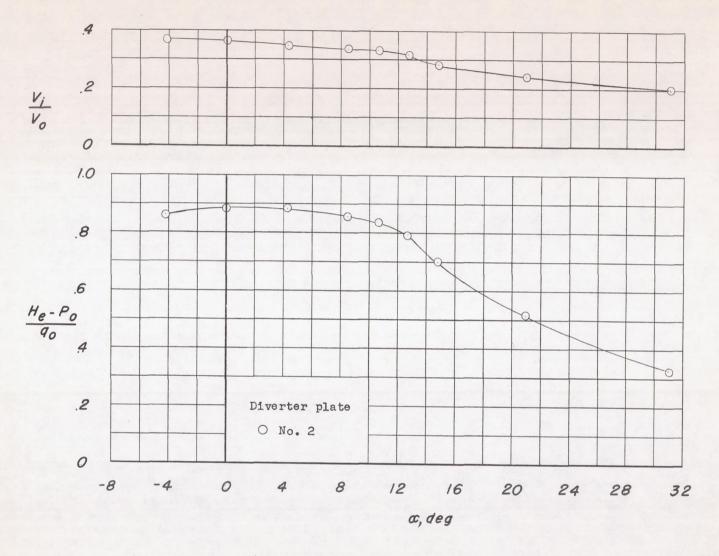
(b) Exit, half open.

Figure 35.- Concluded.



(a) Exit, full open.

Figure 36.- Variation of $\frac{V_1}{V_0}$ and $\frac{H_e - P_o}{q_o}$ with angle of attack for the model equipped with inlet D₁ and horizontal tail T. $\frac{1}{28}$. R = 9 × 10⁶.



(b) Exit, 39 percent open.

Figure 36.- Concluded.

